

# Radio-optical analysis of extended radio sources in the First Look Survey field

Cláudio Moisés Paulo Hons., B.Sc.(Hons)

A thesis submitted in partial fulfillment of the requirements for the degree of Magister Scientiae in the Department of Physics, University of the Western Cape.



**Supervisor: Prof. Catherine Marion Cress**

March 8, 2010

# Radio-optical analysis of extended radio sources in the First Look Survey field

Cláudio Moisés Paulo

## Keywords

radio astronomy

sub-mJy population

telescopes: WSRT, VLA, GMRT

Spitzer FLS field

optical identification

galaxies: active

galaxies: distances and redshifts

galaxies: evolution

galaxies: high-redshift

galaxies: jets



# Abstract

Radio-optical analysis of extended radio sources in the First Look Survey field

C. M. Paulo

MSc thesis, Department of Physics, University of the Western Cape

I combine 610 MHz Giant Metrewave Radio Telescope (GMRT) data, 1.4 GHz Very Large Array (VLA) data and 1.4 GHz Westerbork Synthesis Radio Telescope (WSRT) observations, encompassing a  $\sim 4$  square degree field (sq. deg. field) centred on the verification strip of the Spitzer First Look Survey (FLS) field (RA =  $17^h 18^m 00^s$ , Dec =  $59^\circ 30' 30''$ ), to study radio sources down to fluxes of about 0.1 mJy. The results of an analysis of a sample of 107 multi-component radio sources obtained by cross-correlating the VLA and GMRT catalogues are shown. The spectral index analysis shows that the majority of multi-component sources are steep-spectrum sources. Nevertheless the spread in the spectral distribution is wide, with a significant number of ultra-steep, flat or inverted sources. By cross-correlating 107 multi-component radio sources with the optical catalogues of Marleau et al. (2007) and Papovich et al. (2006), 23 objects were identified and spectroscopically classified as galaxies. Some of them are classified as star-forming or star-burst galaxies, perhaps indicating that AGN and star-formation activity are ongoing in the same galaxy. The measured redshifts span the range  $0 < z < 1.8$  and peak at  $z \sim 0.2$ . According to their radio power ( $P$ ), 6 of the identified objects are in the range of FR II sources ( $P_{1.4GHz} > 10^{24.5} W/Hz$ ) while 17 are in the range of FR I sources ( $P_{1.4GHz} < 10^{24.5} W/Hz$ ). Most of the sources having  $P_{1.4GHz} < 10^{24.5} W/Hz$  are compact and few are extended and peculiar, while all sources in the range of  $P_{1.4GHz} > 10^{24.5} W/Hz$  are extended. Further optical follow-up is recommended to allow a more complete census of the sub-mJy population and more information on AGN feedback from such sources.

March 8, 2010

## Declaration

I declare that *Radio-optical analysis of extended radio sources in the First Look Survey field* is my own work, that it has not been submitted for any degree or examination in any other university, and that all the sources I have used or quoted have been indicated and acknowledged by complete references.

Cláudio Moisés Paulo

Signed: .....



March 8, 2010



## Acknowledgments

I wish to thank the Square Kilometer Array (SKA) South Africa for giving me an opportunity to register for an MSc in Astrophysics. I wish to thank my supervisor Prof. Catherine Marion Cress for patiently guiding and supporting me throughout this thesis as well as Dr. Prandoni and Prof. Morganti for help and encouragement. In addition, I wish to dedicate special thanks to the UWC astrophysics research group for always being there to listen to my questions. Their encouragement, friendship and mentor-ship can indeed be seen through this thesis. Lastly, I wish to thank my mother for giving me life, my fiancé Gina for her unconditional support and encouragement since the day we met.



---

# Contents

---

Keywords . . . . .	i
Abstract . . . . .	ii
Declaration . . . . .	iii
Acknowledgments . . . . .	iv
<b>1 Introduction</b>	<b>2</b>
1.1 Relevance of the project to the Square Kilometre Array . . . . .	3
<b>2 Literature review</b>	<b>5</b>
2.1 Astronomical Facilities . . . . .	5
2.1.1 Spitzer Space Telescope . . . . .	5
2.1.2 Very Large Array Telescope . . . . .	8
2.1.3 Westerbork Synthesis Radio Telescope . . . . .	9
2.1.4 Giant Metrewave Radio Telescope . . . . .	10
2.1.5 The WIYN Observatory . . . . .	11
2.1.6 The MMT Observatory . . . . .	12
2.2 Radio sources . . . . .	13
2.3 Types of radio sources . . . . .	15
2.3.1 Supernovae remnants . . . . .	15
2.3.2 Pulsars . . . . .	16
2.3.3 Active Galactic Nuclei . . . . .	17
2.3.4 Star-forming galaxies . . . . .	23
2.4 Synchrotron Radiation . . . . .	23
2.5 Deep Radio Surveys . . . . .	25
2.6 Spectral index . . . . .	26
2.7 The Spitzer First Look Survey . . . . .	28
2.8 Optical Identifications of radio sources . . . . .	29
2.8.1 Matching techniques . . . . .	30

<b>3</b>	<b>Methodology</b>	<b>36</b>
3.1	Data . . . . .	36
3.2	Methods . . . . .	39
3.2.1	Cross-correlation of radio catalogues and spectral index derivation	39
3.2.2	Optical identification . . . . .	40
3.2.3	Derivation of radio and optical luminosity . . . . .	43
<b>4</b>	<b>Results and Discussion</b>	<b>44</b>
4.1	Cross-correlation of radio catalogues and morphological classification of sources in the FLSv . . . . .	44
4.2	The radio spectral index . . . . .	51
4.3	Optical identification of the FLSv radio sources . . . . .	52
4.4	Luminosity and classification of sources optical identified in the FLSv .	56
<b>5</b>	<b>Conclusions and recommendations</b>	<b>68</b>
	<b>References</b>	<b>70</b>



---

## List of Figures

---

Figure 2.1	The Space Infrared Telescope Facility. Credit: <a href="http://www.spitzer.caltech.edu">http://www.spitzer.caltech.edu</a>	6
Figure 2.2	Very Large Array Telescope. Credit: <a href="http://www.vla.nrao.edu/">http://www.vla.nrao.edu/</a>	8
Figure 2.3	Westerbork Synthesis Radio Telescope.	10
Figure 2.4	Illuminated GMRT antennas at twilight.	11
Figure 2.5	WIYN 3.5 <i>m</i> Telescope - Kitt Peak.	12
Figure 2.6	The 6.5 <i>m</i> MMT telescope.	13
Figure 2.7	Andromeda galaxy on the left: Credit: <a href="http://spot.pcc.edu/~gvershum/">spot.pcc.edu/~gvershum/</a> . On the right, you see Cygnus A. Credit: <a href="http://www.laeff.inta.es/.../radio/cursorad.php?r=6">www.laeff.inta.es/.../radio/cursorad.php?r=6</a>	14
Figure 2.8	The Crab Nebula: a supernova remnant in the constellation of Taurus. Credit: <a href="http://www.networkddirectory.com/blogs/permalinks/12">www.networkddirectory.com/blogs/permalinks/12</a>	15
Figure 2.9	Left: Schematic view of a pulsar. Credit: <a href="http://www.atnf.csiro.au">http://www.atnf.csiro.au</a> . Right: Composite Optical/X-ray image of the Crab Nebula, showing synchrotron emission in the surrounding pulsar wind nebula, powered by injection of magnetic fields and particles from the central pulsar. Credit: same as Figure 2.8.	17
Figure 2.10	Example of FR Classes of galaxy. Credit: <a href="http://www.absoluteastronomy.com">www.absoluteastronomy.com</a>	20
Figure 2.11	Artist's illustration of Quasar. Credit: <a href="http://ksjtracker.mit.edu/.../">ksjtracker.mit.edu/.../</a>	21
Figure 2.12	Seyfert Galaxy NGC 7742. Credit: Hubble Heritage Team.	22
Figure 2.13	Synchrotron Radiation. Credit: <a href="http://openlearn.open.ac.uk">http://openlearn.open.ac.uk</a>	23
Figure 2.14	Representation of parallel and perpendicular components of $\mathbf{v}$ .	24
Figure 2.15	Coverage of public survey in the FLS field. Credit: Fadda et al. (2006).	29
Figure 3.1	VLA mosaic image of FLSv.	37
Figure 3.2	WSRT mosaic image of FLSv.	37
Figure 3.3	GMRT mosaic image of FLSv.	38
Figure 3.4	Example of overlay between radio and optical image of the FLSv field.	42

Figure 4.1	Example of preliminary classification of the radio source morphology: Fanaroff and Riley Class I/II. . . . .	50
Figure 4.2	Example of preliminary classification of the radio source morphology: WAT. . . . .	51
Figure 4.3	Spectral index. . . . .	51
Figure 4.4	Positions of optical identified sources in the FLSv. . . . .	55
Figure 4.5	Redshift distribution of sources optical identified in the FLSv field. . . . .	55
Figure 4.6	Optical luminosity versus radio power of sources optical identified in the FLSv. . . . .	58
Figure 4.7	Radio images of sources having $P_{1.4GHz} < 10^{24.5} W/Hz$ . . . . .	61
Figure 4.8	Continuation of Figure 4.7. . . . .	62
Figure 4.9	Continuation of Figure 4.7. . . . .	63
Figure 4.10	Radio images of sources having $P_{1.4GHz} > 10^{24.5} W/Hz$ . . . . .	64
Figure 4.11	Overlay between radio sources optical identified and some deep NOAO optical image of the FLS field. . . . .	66



---

## List of Tables

---

Table 2.1	Quick facts about Spitzer telescope. . . . .	6
Table 2.2	Array configuration of VLA. . . . .	9
Table 2.3	Spectral index ( $\alpha$ ). Credit: Prandoni et al. (2006). . . . .	27
Table 3.1	Area observed, resolution, sensitivity and sources detected by VLA, WSRT and GMRT in the FLS field. . . . .	38
Table 4.1	Radio multi-component sources cross - identified between VLA and GMRT catalogues. . . . .	46
Table 4.2	Continuation of Table 4.1. . . . .	47
Table 4.3	Continuation of Table 4.1. . . . .	48
Table 4.4	Continuation of Table 4.1. . . . .	49
Table 4.5	Statistical information on spectral index ( $\alpha$ ) properties for multi-component sources in the FLSv field. . . . .	52
Table 4.6	Optical identified multi-component sources of FLSv. . . . .	54
Table 4.7	Information about: radio luminosity, optical luminosity and classification of sources optical identified in the FLSv. . . . .	57
Table 4.8	Source name of the images in Figures 4.7, 4.8, 4.9 and 4.10. . . . .	60

Deep radio observations offer one of the most important windows on the evolution of star formation and black-hole-related activity as a function of cosmological epoch (Owen et al., 2005). Combining Radio, Optical/Near Infrared (NIR), Far Infrared (FIR) and X-ray data have the potential to give us a well-constrained picture of our Universe (Owen et al., 2005).

A small region of the First Look Survey (FLS) field (the verification strip) has been imaged very deeply (Morganti et al., 2004), and is well studied in different wavebands, therefore providing enough information to derive the radio spectral index but also to construct the spectral energy distribution for all the sources where Optical, IR etc. data are available.

Note that the identification of radio sources has turned out to be one of the most productive techniques for discovering new and important classes of astrophysical objects (Lilly and Longair, 1984) over the last 3 decades. This is important for two reasons. Firstly, it is not possible from the radio measurements alone to determine the distance to a radio source. Only if there is an optical identification can the redshift and the distance be determined. Using Hubble's Law it is then possible to calculate the absolute radio luminosity, linear size, and energy content from measurements of radio flux density and angular structure. Secondly, optical as well as x-ray and infrared studies of the radio source counterparts may give some insight into the nature of the intense radio emission (Kellermann and Owen, 1988).

In this thesis, I make use of the existing radio survey data obtained from the Very Large Array (VLA), Giant Metrewave Radio Telescope (GMRT) and Westerbork Synthesis Radio Telescope (WSRT) in combination with data at other wavelengths of this region, encompassing a  $\sim 4$  square degree field (sq. deg. field), centred on the verification strip, to understand the sub-mJy radio population (a mixture of star-forming galaxies and Active Galactic Nucleus (AGNs)). Of particular interest is the possibility of assessing whether its AGN component is more related to efficiently accreting systems (for example radio-intermediate/quiet quasars) or to systems with very low accretion rates (for example FRI radio galaxies (Fanaroff and Riley, 1974)). Such a study may also give important clues on the relative contribution of radiative versus jet-driven (kinetic) feedback to the global AGN feedback in models of galaxy formation.

Very useful is the availability of data at two radio frequencies, 0.61 and 1.4 GHz, which allowed me to derive the source spectral index ( $\alpha$ ). This is important since different accreting regimes may display different spectral signatures in the radio domain (Prandoni et al., 2009).

The thesis is organised as follows. In chapter 2, I give a brief literature review. In chapter 3, I present the data and describe how the results were produced. In chapter 4, I present and discuss my results. Conclusion and recommendations are given in chapter 5.

## 1.1 Relevance of the project to the Square Kilometre Array

With this project, I gained experience in analysing and interpreting interferometric radio data, which is perhaps the best preparation for the upcoming telescope projects such as MeerKAT, Square Kilometre Array (SKA) and/or other radio astronomy instruments and initiatives. The science itself will also be relevant to SKA, and possibly MeerKAT, depending on the final specifications of those instruments. When I return to Maputo, I will be in a good position to provide support to any radio astronomy



effort which includes Mozambique.

Next year, I plan to teach an introductory Astronomy course to Physics undergraduates in Maputo so we can start building a larger Astronomy community in my country. To publicise opportunities and raise awareness of Astronomy, I organised many events this year around the International Year of Astronomy celebrations in collaboration with Brazilian and Portuguese Astronomers.



---

## Literature review

---

In this chapter, I briefly review some of the main concepts of the study. I start by giving a general information about the astronomical facilities used to get the data for this study. After that, a discussion about the nature of radio sources is given. Finally, I give some background about radio surveys, spectral index studies, the FLS and optical identification of radio sources.

### 2.1 Astronomical Facilities

In this section, I briefly introduce the telescopes used to get the data for this study.

#### 2.1.1 Spitzer Space Telescope

The Spitzer Space Telescope (Figure 2.1) is part of NASA's Great Observatories Program, which is made up of four space-based telescopes which together cover the full-spectrum of light from FIR to gamma-ray radiation. The other three are the Hubble Space Telescope (covering the visible and near-ultraviolet), Chandra X-ray Observatory (soft X-rays), and Compton Gamma Ray Observatory (hard X-rays and gamma rays). The left side of Figure 2.1 shows some key parts of Spitzer Space Telescope and on the right side there is an artist's representation of the telescope. (Tony and Martin, 2009).

The telescope covers the infrared part of the spectrum. Astronomical objects that emit primarily in the infrared are mostly cold, dark objects. To observe these stellar bodies, a telescope's detector must be as cold as possible, as the thermal noise within

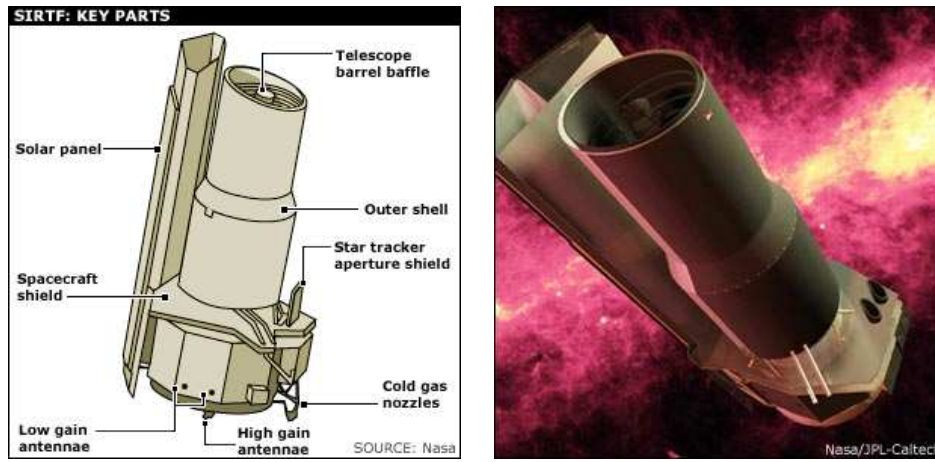


**Figure 2.1:** The Space Infrared Telescope Facility. Credit: <http://www.spitzer.caltech.edu>

the detector itself can otherwise overwhelm the very photons that come from the objects of interest. Spitzer has been peering at those cold cosmic targets by chilling its light detectors to just  $5.5\text{ K}$  using liquid helium, the coldest cryogen available. (Tony and Martin, 2009).

The telescope was launched on August 25th 2003, carrying 360 liters of the cryogen, which was originally meant to last for at least 2.5 years with a hope of stretching it to 5 years. The first major scientific observation carried out with Spitzer was the non proprietary extra-galactic First Look Survey (xFLS) (Frayner et al., 2006). Facts about Spitzer are listed in Table 2.1, including: launch mass, mirror size, Spitzer range of wavelength and instruments (Tony and Martin, 2009). After almost 6 years of the

**Table 2.1:** Quick facts about Spitzer telescope.

Launch mass	950 <i>kg</i>
Mirror size	85 <i>cm</i>
Pass-band ( $\lambda$ )	3.6, 4.5, 5.8, 8.0, 24, 70 160 $\mu\text{m}$
Instruments	IRAC, Infrared Spectrograph, MIPS

cold-phase mission, the cryogen ran out. Even without the cryogen, Spitzers capabilities in the mid-infrared are not expected to degrade at all, as that detector is designed to maintain temperatures below  $30\text{ K}$  even without the liquid helium. These capabilities will not be surpassed by NASA until the James Webb Space Telescope becomes operational after 2013. What the telescope will lose is its ability to see objects in the

far-infrared. Unlike the Hubble, which is in low-Earth orbit, Spitzer orbits around the sun just behind Earth, and cannot be reached by the Shuttle to replenish the supplies and upgrade the instruments. (Tony and Martin, 2009).

To take advantage of the telescopes FIR capabilities, which were enabled by liquid helium, the mission initially focused on the darkest and coldest cosmic targets. Among many other things, it measured the surface temperature distribution on a planet outside of the solar system for the first time, saw hints of newborn planets around other stars, and observed some of the highest-redshift objects ever seen in our universe. (Tony and Martin, 2009).

In the new warm-phase mission, the telescope will still focus on scientific objectives that remain out of reach of any other telescope. It will conduct surveys of the sky to map the universe at extreme distances. Much of the light emitted by such distant galaxies is redshifted to the infrared region. One of the expected results of the new Spitzer survey is the identification of more than a thousand quasars that are at least 12 billion light-years away. (Tony and Martin, 2009).

The warm mission depends on no consumables, and is expected to last for at least 5 more years running until the performance of its on board instruments starts degrading. NASA has already scheduled over 10,000 hours of scientific observations for the first two years of the warm phase mission, and these plans will be executed as soon as it is clear that the telescope behaves as expected without the cryogen. (Tony and Martin, 2009).

Note that one of the main advantages of the Spitzer Space Telescope Facility (SIRTF) is the possibility of making extra-galactic surveys of large regions of the sky in a relatively short time covering wavelengths from the near-IR to the far-IR with the instruments Infrared Array Camera (IRAC) and Multiband Image Photometer (MIPS) (Fadda et al., 2004).

## 2.1.2 Very Large Array Telescope

The Very Large Array Telescope (VLA) is one of the world's premier astronomical radio observatories. It consists of 27 radio antennae in a Y-shape configuration near Socorro, New Mexico. Each antenna is 25 *m* in diameter. Data from the antennae are combined electronically to give the resolution of an antennae 36 *km* across, with the sensitivity of a dish of 130 *m* in diameter. (Robyn, 2009).

The VLA (Figure 2.2) is used primarily by astronomers from around the world. In addition, It is also occasionally used for atmospheric/weather studies, satellite tracking, and other miscellaneous science. (Robyn, 2009).

Table 2.2 shows that there are four configurations of the telescopes. The telescopes



**Figure 2.2:** Very Large Array Telescope. Credit: <http://www.vla.nrao.edu/>

are switched between these configurations approximately every four months. The resolution of the VLA is set by the size of the array. (Robyn, 2009).

The resolution of the VLA is set by the size of the array – up to 36 *km* across. At their highest frequency (43 *GHz*) this gives a resolution of 0.04 arcseconds: sufficient to see a golf ball held by a friend 150 *km* away. (Robyn, 2009).

Its important to know that the Slew rates of the VLA are: 40° per minute in az-

**Table 2.2:** Array configuration of VLA.

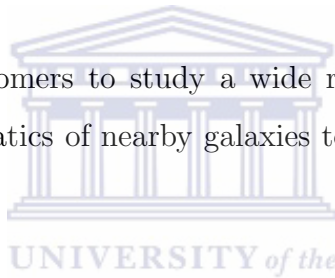
Array configuration	Maximum antenna separation ( <i>km</i> )
A	36
B	10
C	3.6
D	1

imuth and  $20^\circ$  per minute in elevation. The minimum elevation angle is  $8^\circ$  above the horizon and the frequency coverage lies between 74 and 50,000 *MHz*. (Robyn, 2009).

### 2.1.3 Westerbork Synthesis Radio Telescope

The Westerbork Synthesis Radio Telescope (WSRT) is one of the most powerful radio observatories in the world located in the Netherlands (Astron, 2009).

The WSRT, enables astronomers to study a wide range of astrophysical problems: from pulsars and the kinematics of nearby galaxies to the physics of black-holes (Astron, 2009).



Note that the WSRT (Figure 2.3) consists of 14 dish-shaped antennas which operates in frequencies between 115 *MHz* to 8650 *MHz* (Astron, 2009).

According to Astron (2009), the antennas can be individually directed at any point on the sky. Ten of the dishes have a fixed location, while two at the eastern end of the array can be moved on rails. Each antenna has a diameter of 25 *m* (Astron, 2009).

The WSRT is an open user facility available for scientists from any country. It is also part of the European VLBI<sup>1</sup> network (EVN) of radio telescopes (Astron, 2009).

---

<sup>1</sup>Very Long Baseline Interferometry (VLBI) is a type of astronomical interferometry used in radio astronomy. It allows observations of an object that are made simultaneously by many telescopes to be combined, emulating a telescope with a size equal to the maximum separation between the telescopes.



**Figure 2.3:** Westerbork Synthesis Radio Telescope.

### 2.1.4 Giant Metrewave Radio Telescope

The Giant Metrewave Radio Telescope (GMRT), is located at a site about 80 *km* north of Pune, India. GMRT (Figure 2.4) consists of 30 fully steerable gigantic parabolic dishes of 45 *m* diameter each spread over distances of up to 25 *km*. It is one of the most challenging experimental programmes in basic sciences undertaken by Indian scientists and engineers. (Manisha, 2009).

The number and configuration of the dishes was optimized to meet the principal astrophysical objectives which require sensitivity at high angular resolution as well as ability to image radio emission from diffuse extended regions. Fourteen of the thirty dishes are located more or less randomly in a compact central array in a region of about 1 square kilometer (*sq. km*). The remaining sixteen dishes are spread out along the 3 arms of an approximately ‘Y’ - shaped configuration over a much larger region, with the longest interferometric baseline of about 25 *km*. (Manisha, 2009). It is important to know that, the multiplication or correlation of radio signals from all the 435 possible pairs of antennas or interferometers over several hour, enable radio images of celestial objects to be synthesized with a resolution equivalent to that obtainable with a single gigantic dish 25 kilometer in diameter. The array operates in six frequency bands centred around 50, 153, 233, 325, 610 and 1420 *MHz*. All these feeds provide dual polarization outputs. In some configurations, dual-frequency observations are





**Figure 2.4:** Illuminated GMRT antennas at twilight.

also possible (Manisha, 2009).

The highest angular resolution achieves a range from about 60 arcsec at the lowest frequencies to about 2 arcsec at 1.4 *GHz* Manisha (2009).

### 2.1.5 The WIYN Observatory

The WIYN Telescope (Figure 2.5), a 3.5 *m* instrument employing many technological breakthroughs, is the newest and second largest telescope on Kitt Peak (Wyn, 2009).

The WIYN Observatory (pronounced “win ”) is owned and operated by the WIYN Consortium, which consists of the University of Wisconsin, Indiana University, Yale University, and the National Optical Astronomy Observatories (NOAO) (Wyn, 2009).

WIYN instrumentation includes: Mini-Mosaic Imager, Hydra, SparsePak, the Orthogonal Parallel Transfer Imaging Camera (OPTIC) and WIYN High Resolution InfraRed Camera (WHIRC). A multiple object spectrograph employing optical fibers allows the simultaneous observation of the spectra of 100 objects. The imaging cameras employ highly sensitive arrays of electronic detectors. (Wyn, 2009).

The WIYN telescope was used to detect 24  $\mu\text{m}$  and 1.4 GHz sources in the FLS





**Figure 2.5:** WIYN 3.5 *m* Telescope - Kitt Peak.

field using the multifiber spectrograph, Hydra (Wiyun, 2009).

### 2.1.6 The MMT Observatory

The 6.5 *m* Multiple Mirror Telescope (MMT) (Figure 2.6) is operated by the MMT Observatory (MMTO), a joint venture of the Smithsonian Institution and the University of Arizona. The MMT is located on Mt. Hopkins, near Tucson, Arizona. The MMT is on the grounds of the Smithsonian Institution's Fred Lawrence Whipple Observatory. (Pickering, 2009).

The MMT Spectrograph is actually composed of two spectrographs sharing a common focal plane assembly and two filter wheels. The spectrographs are denoted the Blue Channel and Red Channel, after their approximate wavelength bands. (Pickering, 2009).



**Figure 2.6:** The 6.5 m MMT telescope.

## 2.2 Radio sources

The most general definition of an astronomical radio source is simply any astronomical object that radiates electromagnetic energy at radio frequencies (Young, 2002).

We can think of extra-terrestrial radio emissions as originating either within our Galaxy or as extra-galactic. Inside our Galaxy, remnants of supernova explosions and pulsars are strong sources of radio emission (Young, 2002). Outside our Galaxy, we find great variation in the radio emission from different galaxies. We have arbitrarily divided these other galaxies into “normal ” and “active ” galaxies, depending on whether they emit radio emission (Young, 2002).

Normal galaxies are not very strong radio sources. For example, the Great Andromeda Spiral (Figure 2.7, left panel), the largest galaxy in our so-called local group of galaxies, emits  $10^{23}$  watts of power. In contrast, Cygnus A (Figure 2.7, right panel), over half a billion light years from Earth, is one of the most conspicuous radio sources in the sky, with a power output of  $10^{38}$  watts (Young, 2002).

According to Rohlfs and Wilson (2003), active galaxies include radio galaxies, quasars, Seyfert Galaxies and BL Lacertae objects. Note that astronomers are now investigat-

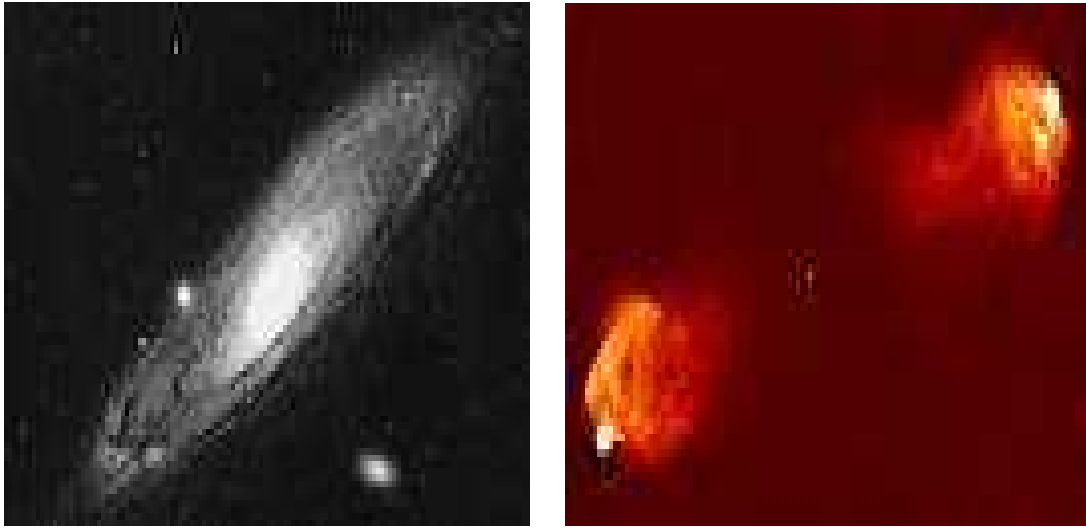


**Figure 2.7:** Andromeda galaxy on the left: Credit: [spot.pcc.edu/~gvershum/](http://spot.pcc.edu/~gvershum/). On the right, you see Cygnus A. Credit: [www.laeff.inta.es/.../radio/cursorad.php?r=6](http://www.laeff.inta.es/.../radio/cursorad.php?r=6)

ing the plausibility of a “unified theory of active galaxies”. It is believed that these galaxies have a super-massive black hole at their centers, and their appearance to us depends on the angle at which we are observing them (Young, 2002).

Radio galaxies reveal some of the most dramatic physical events ever seen, and they provide essential clues to the basic evolutionary tracks followed by all galaxies. Extragalactic radio sources encompass the largest and the most energetic single entities in the universe (Young, 2002).

Most radio sources show evidence for jets, that is, elongated features which emanate from the nucleus ending in one of the regions of extended emission (Rohlfis and Wilson, 2003). The predominant radiation-producing mechanism is synchrotron radiation (Young, 2002). Many astronomers are now investigating the connection between active Galaxies and star-forming Galaxies.

## 2.3 Types of radio sources

### 2.3.1 Supernovae remnants

A Supernova remnant (SNR) is the remains of a supernova explosion (SNe<sup>2</sup>). Its appearance (Figure 2.8) depends on: (i) its age; (ii) the type of supernova; (iii) whether it contains a pulsar that can provide a continuing source of energy to all or a part of the remnant; and (iv) the density of the local interstellar medium (Lyne et al., 1998). SNRs are extremely important for understanding our Galaxy. They heat up

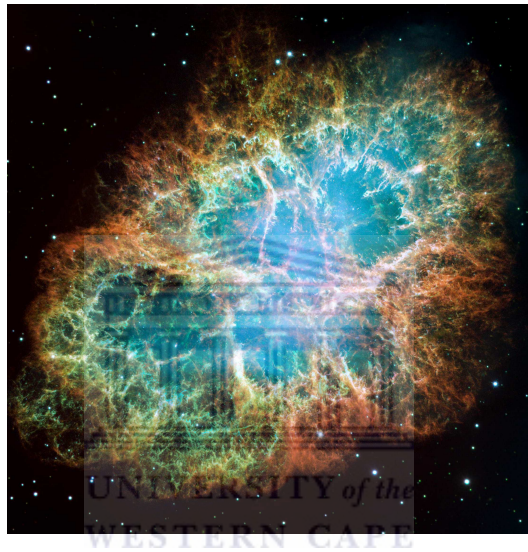


**Figure 2.8:** The Crab Nebula: a supernova remnant in the constellation of Taurus. Credit: [www.networlddirectory.com/blogs/permalinks/12](http://www.networlddirectory.com/blogs/permalinks/12)

the interstellar medium, distribute heavy elements through the Galaxy, and accelerate cosmic rays (Pickering, 2009).

There are various types of SNR: simple Shell-type remnants with nothing in their centers; Crab-like remnants or plerions with pulsars in their centers; and Composite remnants which is a combination of the first two (NASA, 2009).

Most of the SNRs known in the Galaxy have only been detected at radio frequencies. The reason for this is absorption in the Galactic plane at both optical and X-ray

---

<sup>2</sup>A SNe is the instantaneous release of  $10^{51}$  ergs of energy, the result of either the catastrophic collapse of a massive star or runaway nuclear burning on the surface of a white dwarf.

wavelengths. All available evidence suggests that the shock fronts which accompany SNRs accelerate enough cosmic rays to GeV energies to produce readily detectable radio emission. This is fortunate, as it enables us to study remnants throughout the Galactic disk. Cosmic rays and the magnetic fields in which they gyrate are the essential ingredients for producing the synchrotron radiation which is observed at radio frequencies. (McCray and Wang, 1996).

### 2.3.2 Pulsars

Radio pulsars (Figure 2.9) are rotating neutron stars that emit beams of radio-waves from regions above their magnetic poles (Young et al., 1999). The first pulsar was discovered by chance by Jocelyn Bell and Anthony Hewish in 1967 who were studying distant galaxies at the time and is now called PSR B1919+21<sup>3</sup>. Even though pulsars were first discovered as radio sources they have now been observed using optical, X-ray and gamma-ray telescopes (Maryam, 2009).

Essentially, pulsars are the collapsed cores of massive stars. They are composed of an iron crust which covers incredibly dense neutron star. Pulsars also have a very strong magnetic field, probably with a dipole form, like a bar magnet. Beams of radiation are formed at the magnetic poles, probably directed radially away from the star. As the pulsar rotates, these beams sweep around 360 degrees like a lighthouse. Radio telescopes receive a regular train of pulses as the beam repeatedly crosses the Earth, making the pulsar appear to be a pulsating radio signal (Maryam, 2009). The time interval between consecutive pulses is called the pulsar's period. Periods of one second are typical although pulsars have been discovered with periods from a few milliseconds up to eight seconds. The time between pulses is incredibly regular and can be measured very precisely. Despite their precision, pulsar periods are not constant. At least in their own frame of reference, all pulsars are very gradually losing rotational energy and slowing down. This is attributed to the energy required for the acceleration of relativistic particles and the electromagnetic radiation frequency caused by the strong

---

<sup>3</sup>PSR stands for Pulsating Source of Radio and B1919+21 indicates the position of the pulsar in the sky.

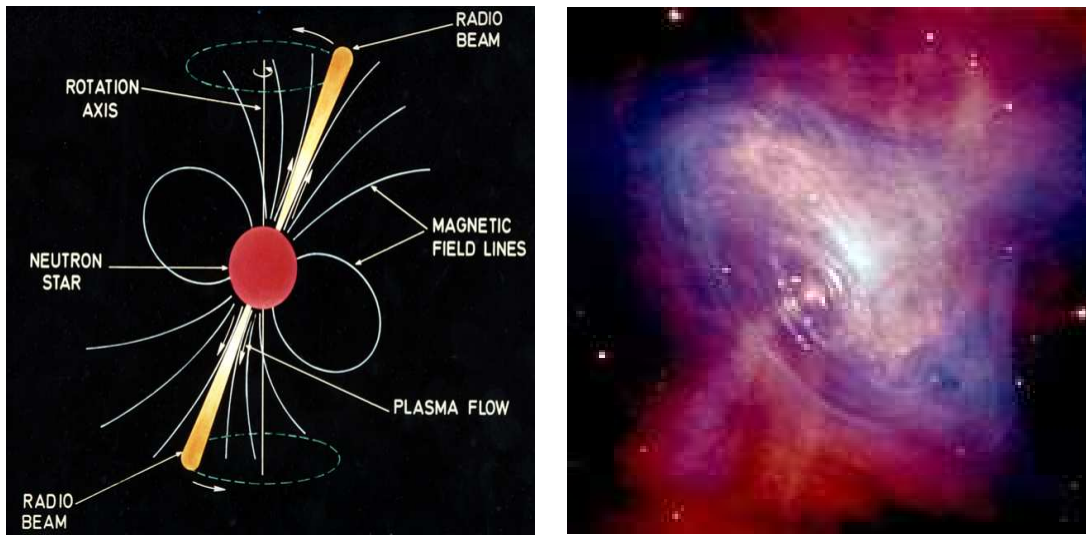


**Figure 2.9:** Left: Schematic view of a pulsar. Credit: <http://www.atnf.csiro.au>. Right: Composite Optical/X-ray image of the Crab Nebula, showing synchrotron emission in the surrounding pulsar wind nebula, powered by injection of magnetic fields and particles from the central pulsar. Credit: same as Figure 2.8.

magnetic field. (Maryam, 2009).

According to Smits et al. (2008), pulsars are useful for studying the Milky Way, globular clusters, the evolution and collapse of massive stars, the formation and evolution of binary systems, the properties of super-dense matter, extreme plasma physics, tests of theories of gravity, the detection of gravitational waves, and astrometry, to name only a few areas. Indeed, many of these areas of fundamental physics can be best – or even only – studied, using radio observations of pulsars (Smits et al., 2008).

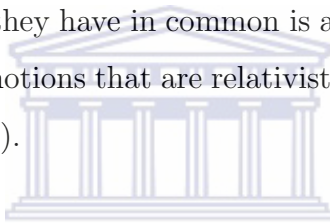
To harvest the information and science accessible through pulsar observation, two different types of observations are required. Firstly, suitable pulsars need to be discovered via radio surveys that sample the sky with high time and frequency resolution. Secondly, after the discovery, a much larger amount of observing is required to extract most of the science using pulsar timing observations. (Smits et al., 2008).

### 2.3.3 Active Galactic Nuclei

Active galactic nuclei, are galaxies with a compact central region (nucleus), from which we observe substantial radiation that is not the light of stars or emission from the gas heated by them (Sparke and Gallagher, 2007). Active nuclei emit strongly over the

whole electromagnetic spectrum, including the radio, X-ray, and  $\gamma$ -ray regions where most galaxies hardly radiate at all. AGNs are divided into two classes: radio-quiet and radio-loud. Low-ionization nuclear emission-line regions, Seyfert galaxies and radio-quiet quasars are examples of radio-quiet AGNs and radio-loud quasars, blazars and radio galaxies are examples of radio-loud AGNs. The most powerful of them, the quasars, easily outshine their host galaxies. With luminosities exceeding  $10^{12}L_{\odot}$ , many are bright enough to be seen most of the way across the observable Universe. But the emitting region may be no bigger than the solar system; its power source is probably the energy released by gas falling into a central black hole. (Sparke and Gallagher, 2007).

Many galactic nuclei are very luminous at optical, ultraviolet, and X-ray wavelengths. Others are far dimmer than their host galaxies in these spectral regions, but are strong radio sources. What they have in common is a large energy output from a very small volume, and internal motions that are relativistic, with speeds greater than  $0.1c$ . (Sparke and Gallagher, 2007).



While very luminous AGN can be unambiguously identified in almost any energy band, AGN become progressively more challenging to identify at lower luminosities when their emission may be equal or even substantially less than that of their host galaxy. These lower-luminosity AGN are important to identify, and thus maximize samples of AGN for demographic studies. (Arnold and Martini, 2009).

According to Koulouridis et al. (2009), the lack of detailed knowledge of key aspects of the AGN mechanism leaves us with many scattered pieces of information. Theory is unable to explain observations in most cases, and observations cannot resolve the galactic nuclei to confirm theories (Koulouridis et al., 2009).

## Radio Galaxies

Galaxies which are identified with strong radio sources in the range of  $10^{41}$  to  $10^{46}$  *ergs s*<sup>-1</sup> are generally referred to as “radio galaxies”.



For the most part, radio galaxies are giant ellipticals with absolute visual magnitude about  $-21$ . They often exhibit jet structure from a compact nucleus. They typically exhibit two lobes of radio frequency emission that are often approximately aligned with the jets observed in the visible spectrum and which can be as large as 1Mpc in size.

Among the most energetic phenomena in the universe, radio galaxies are excellent laboratories in which we can investigate some of the major challenges of today’s astrophysics, such as accretion onto super-massive black holes (SMBH), the associated formation of relativistic jets, the feedback processes of an “active” SMBH in the star formation history of a galaxy and the role of the AGN in injecting energy in the intracluster medium (Fanaroff and Riley, 1974).

Radio galaxies have been historically classified according to their radio morphology, following the Fanaroff and Riley (1974) criteria: a FR I source has bright jets rising from the nucleus, while a FR II has two bright hot spots far from it. They also noted that FR II are mostly found at high radio luminosities, while FR I are associated with weaker radio sources. An example of Fanaroff and Riley classes is shown in Figure 2.10. The left panel of Figure 2.10 shows an image of the large-scale radio structure of the FR I radio galaxy 3C31. The Jets and plumes are labelled. The right panel shows an image of the large-scale radio structure of the FR II radio galaxy 3C98. The lobes, jet and hot-spot are labelled. The two FR classes also differ, at least statistically, in several other properties, such as the environment and host luminosities (Buttiglione et al., 2009). However, it soon became apparent that the transition between the two classes is continuous and objects of intermediate radio structure do exist. The FR I/FR II break (at low redshifts) also depends on the luminosity of the host galaxy. From the optical point of view, FR I galaxies are invariably associated with the most massive galaxies in the local universe, thus they are also most likely to be linked with the most massive black holes in the local universe. Furthermore, FR I galaxies are usually located at the center of rich clusters. On the other hand, at low redshifts, FR II galaxies are generally found in regions of lower density, while a few FR II galaxies are found in richer groups or clusters at redshifts higher than  $z \sim 0.5$  (Buttiglione



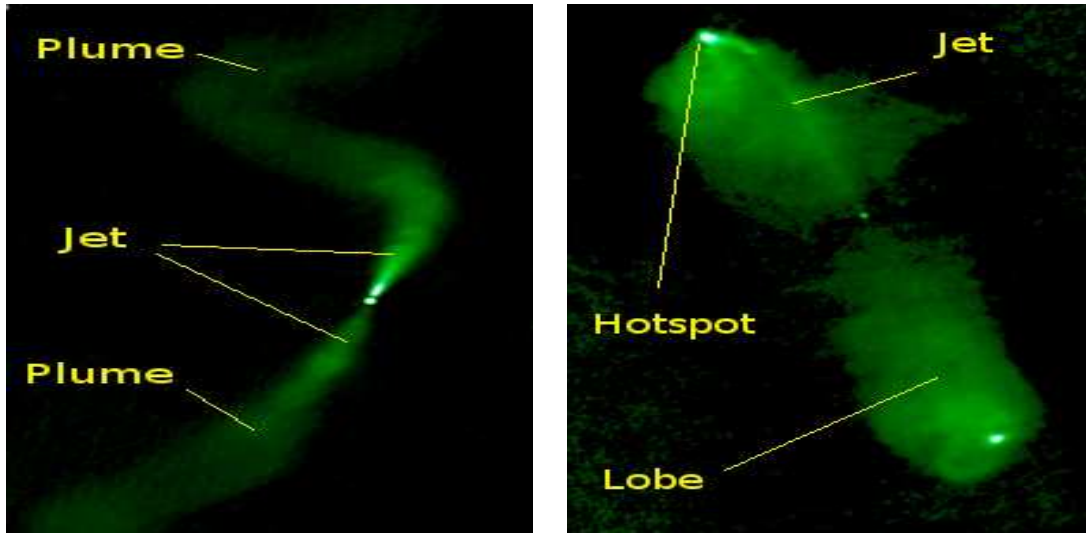


**Figure 2.10:** Example of FR Classes of galaxy. Credit: [www.absoluteastronomy.com](http://www.absoluteastronomy.com)

et al., 2009).

According to their morphology, radio galaxies can also be classified as compact, extended, peculiar, wide-angle tail (WAT), etc. For example, Kantharia et al. (2009) WAT galaxies are a subset of radio galaxies near the Fanaroff and Riley luminosity transition, which have been extensively discussed because of their exclusive association with cluster dominant galaxies and also because of the abrupt flaring of their jets after maintaining a well collimated flow to distances  $\geq 20$  kpc from the core.

## Quasar

A quasi-stellar radio source (quasar - Figure 2.11 ) is a very energetic and distant galaxy with an AGN. They were first discovered with radio telescopes in the late 1950s and many were recorded as radio sources with no corresponding visible object. Quasars reside in a variety of galaxies, from normal to highly disturbed. Optically they appear point-like because the the central region completely outshines the host galaxy. Some quasars display changes in luminosity which are rapid in the optical range and even more rapid in the X-rays. This implies that they are small (Solar System sized or less) because an object cannot change faster than the time it takes light to travel from one end to the other; but relativistic beaming of jets pointed nearly directly toward us explains the most extreme cases. (Willott et al., 2007).



**Figure 2.11:** Artist's illustration of Quasar. Credit: [ksjtracker.mit.edu/.../](http://ksjtracker.mit.edu/.../)

One interesting characteristic of very high-redshift quasars is that they show evidence of elements heavier than helium, indicating that galaxies underwent a massive phase of star formation, creating population III stars between the time of the Big Bang and the first observed quasars.

### Seyfert galaxies

According to Sparke and Gallagher (2007), Seyfert galaxies<sup>4</sup> (Figure 2.12) are a class of galaxies with nuclei that produce spectral line emission from highly ionized gas. These galaxies are characterized by extremely bright nuclei, and spectra which have very bright emission lines of hydrogen, helium, nitrogen, and oxygen (Seyfert, 2007).

Seyfert galaxies, show strong emission in the radio, infrared, ultraviolet, and X-ray parts of the spectrum. The radio emission is believed to be synchrotron emission from the jet. The infrared emission is due to radiation in other bands being reprocessed by dust near the nucleus. The highest energy photons are believed to be created by inverse Compton scattering by a high temperature corona near the black hole. (Haardt and Maraschi, 1991).

Note that Seyferts were first classified as Type 1 or 2, depending upon whether the

<sup>4</sup>Named after Carl Seyfert, the astronomer who first identified the class in 1943 (Seyfert, 2007).



**Figure 2.12:** Seyfert Galaxy NGC 7742. Credit: Hubble Heritage Team.

spectra show both narrow and broad emission lines (Type 1), or only narrow lines (Type 2) (Haardt and Maraschi, 1991). The narrow and broad components are believed to both originate from the accretion disk, but in Type 2 Seyferts it is believed that the broad component is obscured by dust and/or by our viewing angle on the galaxy. In some Type 2 Seyfert galaxies, the broad component can be observed in polarized light; it is believed that light from the broad-line region is scattered by a hot, gaseous halo surrounding the nucleus, allowing us to view it indirectly (Haardt and Maraschi, 1991).

### **BL Lacertae objects**

BL Lacertae objects, or BL Lacs, are classes of AGN that are defined on the basis of their optical spectra (Whiting, 2005) and are viewed along the jets. In contrast to other types of AGN, BL Lacs are characterized by rapid and large amplitude flux variability and significant optical polarization. When compared to the more luminous active nuclei (quasars) with strong emission lines, BL Lac objects have spectra dominated by a featureless non-thermal continuum (Alan et al., 2008).

BL Lacs are believed to be intrinsically identical to low power radio galaxies but with the jet closely aligned to the line of sight of the observer. These active nuclei are hosted by massive spheroidal galaxies. From the point of AGN classification, BL Lacs are a blazar sub-type (Alan et al., 2008).

### 2.3.4 Star-forming galaxies

In star-forming regions of galaxies, there are many supernovae. Charged particles from the supernova remnants interact with the magnetic fields in the ISM to produce synchrotron emission. Dust is also formed in star-forming regions and can produce thermal radio emission. 'Normal' galaxies like the Milky Way are thus low-power radio sources. Star-bursting galaxies are somewhat brighter radio sources and become a significant component of the radio population as one goes fainter than  $\sim 10$  mJy.

## 2.4 Synchrotron Radiation

Synchrotron radiation (Figure 2.13), the emission by relativistic and ultra-relativistic electrons gyrating in magnetic fields, is the process which dominates high energy astrophysics. It was originally observed in early beta-tron experiments in which electrons were first accelerated to ultra-relativistic energies. This process is responsible for the radio emission from the Galaxy, SNRs and extra-galactic radio sources. It is also responsible for the non-thermal optical and X-ray emission observed in the Crab Nebula and possibly for the optical and X-ray continuum emission of quasars. According

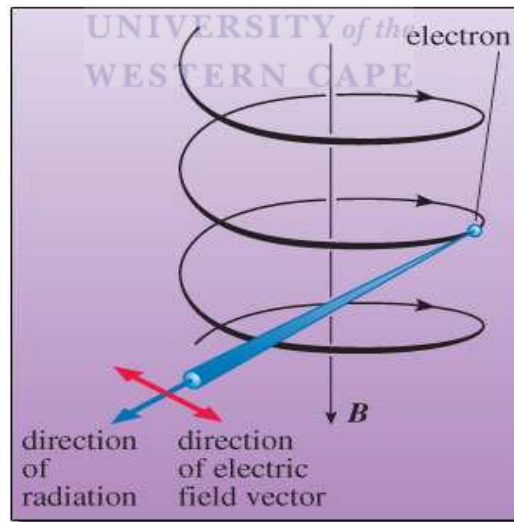


**Figure 2.13:** Synchrotron Radiation. Credit: <http://openlearn.open.ac.uk>

to Rohlfs and Wilson (2003), the motion of a particle with charge  $e$  and mass  $m$  that moves with a velocity  $\mathbf{v}$  in a (homogeneous) magnetic field with the flux density  $\mathbf{B}$  and Lorentz factor  $\gamma$  is governed by the relativistic Einstein-Planck equations

$$\frac{d}{dt}(\gamma m \mathbf{v}) = e(\mathbf{v} \times \mathbf{B}). \quad (2.1)$$

If there is no electric field  $\mathbf{E}$ , then energy conservation results in the additional equation

$$\frac{d}{dt}(\gamma m c^2) = 0. \quad (2.2)$$

But this implies that  $\gamma = (1 - v \cdot v/c^2)^{-1/2}$  is constant and therefore that  $|\mathbf{v}|$  is constant. Projecting  $\mathbf{v}$  into two components,  $\mathbf{v}_{\parallel}$  to  $\mathbf{B}$  and  $\mathbf{v}_{\perp}$  perpendicular to  $\mathbf{B}$  (Figure 2.14), one finds that

$$\frac{d\mathbf{v}_{\parallel}}{dt} = 0 \quad (2.3)$$

and

$$\frac{d\mathbf{v}_{\perp}}{dt} = \frac{e}{\gamma m}(\mathbf{v}_{\perp} \times \mathbf{B}). \quad (2.4)$$

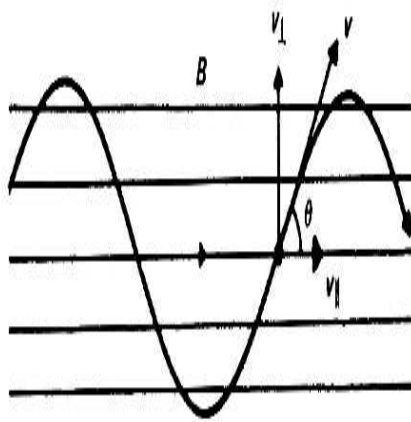


**Figure 2.14:** Representation of parallel and perpendicular components of  $\mathbf{v}$ .

Equation 2.3 has the solution  $\mathbf{v}_{\parallel} = \text{constant}$  so that, since  $|\mathbf{v}|$  is constant,  $|\mathbf{v}_{\perp}|$  must also be constant. The solution to 2.4 therefore must obviously be uniform circular motion with a constant orbital velocity  $v_{\perp} = |\mathbf{v}|$ . The frequency of the gyration is

$$\omega_G = \frac{eB}{\gamma m}. \quad (2.5)$$

Since the constant velocity  $\mathbf{v}_{\parallel}$  is superimposed on this circular motion, the path followed by the electron is a helix winding around  $\mathbf{B}$  with the constant pitch angle

$$\tan \theta = \frac{\mathbf{v}_{\perp}}{\mathbf{v}_{\parallel}} \quad (2.6)$$

Inserting numerical values for  $e$  and  $m$ , we find

$$\frac{\omega_G}{MHz} = 17.6 \left( \frac{B}{Gauss} \right) \quad (2.7)$$

So that, for  $B \simeq 10^{-6}$  Gauss in interstellar space,  $\omega_G=18$  Hz (Rohlfs and Wilson, 2003). For a relativistic particle with  $\gamma > 1$ ,  $\omega_B$  will be even smaller! From (2.4) one sees that the electron is accelerated in its orbit, this acceleration is directed perpendicular to  $B$ . Since the electron is accelerated, it will radiate and the total power radiated is

$$P = \frac{2e^4(v_{\perp})^2 B^2}{3m^2 c^3} \left( \frac{E}{mc^2} \right)^2. \quad (2.8)$$

## 2.5 Deep Radio Surveys

Surveys can be defined as extensive observations of regions of sky. They are generally performed for the production of an astronomical catalogue for specific types of astronomical object and usually restricted to one band of the electromagnetic spectrum. Over the last ten years it has become commonplace to conduct surveys that join together different observations of a given region of the sky, obtained with different telescopes at different wavelengths. The first radio sky survey was conducted by Grote Reber and was completed in 1941 (Kraus, 1988).

According to Owen et al. (2005), deep radio observations offer one of the most important windows on the evolution of star-formation and black-hole-related activity as a

function of cosmological epoch. Combining Radio, optical/NIR, FIR and X-ray data have the potential to give us a well constrained picture of the Universe. Each window, by itself, has serious weaknesses. The optical/NIR window is the best studied and provides the most direct view. However, it suffers from uncertainties due to dust obscuration, which is a fundamental part of star-formation (Owen et al., 2005).

FIR observations give us an indirect signal from the dust, but leave uncertainties in the origin of the heating of the dust and we fail to see into the heart of the AGN or star-forming regions. In X-ray and radio observation we can see behind the dust, but we are measuring secondary emission which is not easy to physically relate to the black hole or star-formation rate (SFR). Thus we need a combination of all this information to form a full picture (Owen et al., 2005).

Radio surveys have the advantage that they are feasible from the ground (like optical) and the observations can be done 24 hours per day. Interferometry allows high-resolution images to be made at radio wavelengths. Mosaicing<sup>5</sup> techniques enable deep observation of a wide field. Figures 3.1, 3.2 and 3.3 in chapter 3 show fields in deep radio surveys.

Surveys enable statistical studies of various source populations and studies related to cosmological evolution. In addition, they make serendipitous discoveries possible.

## 2.6 Spectral index

A spectral index, is a measure of the way in which the intensity of the continuum emission from radio source varies with frequency (Dictionary, 2009). It is calculated from an assumed power law dependence for flux given by:

$$S \propto \nu^\alpha \tag{2.9}$$

---

<sup>5</sup>Combination of regularly spaced multiple pointings linearly combined to produce an image larger than the telescope's primary beam.

where  $S$  is the flux and  $\nu$  is frequency. The index is calculated using

$$\alpha = \frac{\log(S_1/S_2)}{\log(\nu_1/\nu_2)} \quad (2.10)$$

According to the values of  $\alpha$  (Table 4.3), various radio sources can be separated: ultra steep-spectrum sources; steep-spectrum sources; flat spectra-spectrum sources and inverted-spectrum sources. Note that it is possible to combine the spectral index

**Table 2.3:** Spectral index ( $\alpha$ ). Credit: Prandoni et al. (2006).

Spectral index	Designation
$\alpha < -1.3$	Ultra Steep-Spectrum Sources
$-1.3 < \alpha < -0.5$	Steep-Spectrum Sources
$-0.5 < \alpha < 0$	Flat-Spectrum Sources
$\alpha > 0$	Inverted-Spectrum Sources

information with other observational properties and infer the nature of the faint radio population (Mignano et al., 2008).

Very steep radio spectral indices tend to identify the population of Ultra Steep Spectrum sources (USS), which are mostly radio-loud galaxies set at substantial redshifts (Magliocchetti et al., 2007; Miley and De Breuck, 2008). Indeed, objects with high values of  $\alpha$  are typically investigated to look for very high redshift radio galaxies (Magliocchetti et al., 2007; Miley and De Breuck, 2008).

A number of previous studies can be found in the literature which try to explain the presence of systems with very steep spectral slopes at high redshifts. For instance, by comparing the extremely steep spectral index sources associated with galaxies residing closest to the cluster centers, Klammer et al. (2006) found that steeper spectra can be explained by pressure-confined radio lobes which have slow adiabatic expansion losses in high-density environments. Alternatively, one can attribute the steepening of the radio spectrum at low frequencies as due to the scattering between cosmic microwave background (CMB) photons and relativistic electrons at  $z \sim 2$  where the CMB energy density is significantly higher than it is at later epochs (Magliocchetti et al., 2007).



## 2.7 The Spitzer First Look Survey

The Spitzer First Look Survey was a service to the Spitzer user community, initiated as a Director’s Discretionary Time program. It was designed to provide a characteristic deeper first-look at the mid-infrared sky to sensitivities that are two orders of magnitude deeper than previous large-area surveys (Fang et al., 2004), in order to accurately characterize the dominant IR source population.

The public FLS includes three components, described on Spitzer’s website<sup>6</sup>. Here, we focus on the extra-galactic component, whose field was chosen to have low Galactic background and to be in the Spitzer continuous viewing zone (CVZ) such that it would be observed shortly after the Spitzer in-orbit checkout regardless of launch date. The extra-galactic component consisted of shallow observations of 4.4 sq. deg. field, centred at  $\alpha(2000) = 17^h18^{mm}00^s$ ,  $\delta(2000) = 59^\circ30'00''$  (Marleau et al., 2007) and a smaller  $\sim 0.75^\circ \times 0.3^\circ$  strip, referred to as the “verification” survey region (or FLSv) (Morganti et al., 2004). The FLSv observations lie within the shallow survey region, and are centred at  $\alpha(2000) = 17^h117^{mm}00^s$ ,  $\delta(2000) = 59^\circ45'00''$ .

Complementary observations have been taken at a range of wavelengths to fully exploit the new deep infrared data as shown in Figure 2.15 (Garn et al., 2007), therefore providing enough information to derive the radio spectral index ( $\alpha$ ) but also to construct the spectral energy distribution for all the sources where optical, IR, etc. data are available. From the outside going toward the center in Figure 2.15 one sees: (1) KPNO  $R$  images (Fadda et al., 2004), (2)  $24 \mu m$  main field (Fadda et al., 2006), (3) VLA  $20 cm$  (Condon et al., 2003), (4) IRAC channels 1 and 3 (Lacy et al., 2005), (5) IRAC channels 2 and 4 (Lacy et al., 2005), (6) WSRT  $20 cm$  (Morganti et al., 2004), (7)  $24 \mu m$  verification field (Fadda et al., 2006), (8) HSTACS data (L. J. Storrie-Lombardi et al. in preparation). Regions similar to the  $24 \mu m$  one have also been covered at 70 and  $160 \mu m$  (Frayer et al., 2006). In addition to the radio surveys of the FLS field shown in Figure 2.15 made by Condon et al. (2003) using the VLA at 1.4 GHz and by Morganti et al. (2004) using WSRT, there is also the 610 MHz radio survey of this field

<sup>6</sup><http://ssc.spitzer.caltech.edu/fls>

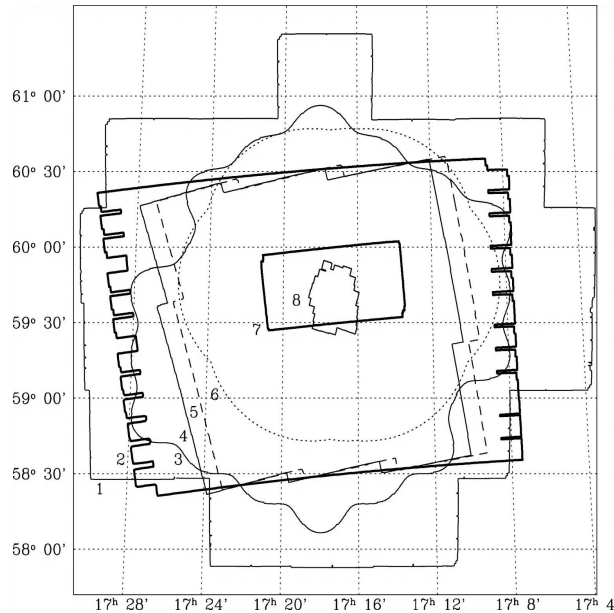


**Figure 2.15:** Coverage of public survey in the FLS field. Credit: Fadda et al. (2006).

made with the GMRT by Garn et al. (2007). The extra-galactic region was covered also by the early data release of the Sloan Digital Sky Survey (SDSS) Stoughton et al. (2002). Further redshift surveys targeting selected  $24 - \mu m$  and/or 1.4 GHz sources were made with the MMT/Hectospec fiber spectrograph and WIYN/Hydra (Papovich et al., 2006; Marleau et al., 2007). These provide the data for this project and are discussed further in chapter 3.

## 2.8 Optical Identifications of radio sources

Here, I give some information's about the history and techniques used for the optical identification of radio sources. Note that the most important of the early identifications were those of the two brightest radio sources in the northern sky, Cassiopeia A and Cygnus A. Interferometry by Smith (1951, 1952) at Cambridge resulted in accurate radio positions for these sources and subsequent optical observations by Baade and Minkowski (1954) led to their identification with very faint optical objects (Lilly and Longair, 1984).

### 2.8.1 Matching techniques

There are several techniques which could be used to cross-correlate radio and optical catalogues. One statistically robust method is the likelihood ratio ( $LR$ ) technique of Sutherland and Sanders (1992). This method is defined as the ratio between the probability that the source is the correct identification and the corresponding probability that the source is a background, unrelated object (Mignano et al., 2008). A threshold value  $L_{th}$  of the likelihood ratio is assumed, above which a counterpart is considered as a good identification and below which is dismissed as spurious (Mignano et al., 2008). The sample of accepted identifications thus consists of all the radio-optical associations that have  $LR > L_{th}$  (Mignano et al., 2008).  $L_{th}$  was chosen to be the value of  $LR$  that maximizes the function  $(C + R)/2$  where  $C$  is the completeness and  $R$  the overall reliability of the sample (Mignano et al., 2008).

Another technique used to cross-correlate radio and optical catalogues is the criteria based on the separation between the sources, which consider as good any identification within a certain fixed radio-optical distance (Mignano et al., 2008). Sutherland and Sanders (1992) demonstrated that the two methods produced very similar catalogues of matched objects in their study. The  $LR$  has been used often in order to identify radio sources. However if the positional accuracies for both radio and optical catalogues are very high, positional coincidence alone can be adequate (Boucheffry and Cress, 2006).

The identification of radio sources continued throughout the 1950s as more accurate positions became available for the fainter sources known at that time. On the Galactic front, many supernova remnants and  $HII$  regions were discovered which were highly obscured or unobservable in the optical waveband. On the extra-galactic front, it was found that many of the early identifications were giant elliptical galaxies, many of them being the brightest galaxies in clusters. The most remarkable result of this period of activity was the discovery in 1960 of quasi-stellar objects (quasars) by Ryle and Sandage (1964) from these optical identification surveys. Since 1960, many quasars have been discovered and it is now appreciated that there is a continuity in nuclear

activity in galaxies all the way from galaxies such as our own, through the Seyfert galaxies to the N-galaxies and quasars. This same optical identification procedure continued to make fundamental contributions to these studies, in particular, with the recognition in 1968 of the class of what are now regarded as probably the most extreme class of quasar-like objects, the BL Lac objects. In the case of BL Lac and other members of this class, the optical spectra are almost featureless and it may be that in these sources the nucleus itself is being observed more or less unobscured by surrounding gas. Another remarkable discovery which has come from the ability of the radio identification technique to find quasars in large numbers has been the discovery of gravitational lenses. (Lilly and Longair, 1984).

Prandoni et al. (2001) optically identified sources in the ATESP<sup>7</sup>-EIS Sample. A search circle of 3'' radius, centred at each radio position, was chosen; this turned out to be a good compromise when inspecting Figure 1 of Prandoni et al. (2001), where the distance distribution of the radio-optical associations with  $I < 22.5$  is present. For double and triple radio sources the distance to the nearest optical counterpart was computed from the radio centroid, while for complex radio sources the distance was computed from the radio peak position. Since this position does not generally coincide with the position of the source nucleus they allowed for distances larger than 3'' and checked for the actual existence of optical counterpart by visual inspection of the radio-optical finding charts. As to the radio morphology, among 386 sources three are triples (none identified), three are complex (one identified), twenty-one are doubles (six identified) and 359 are point-like (212 identified).

In 2002, Ivezić et al. (2002) discussed the optical and radio properties of  $\sim 30,000$  FIRST (radio, 20 cm, sensitive to 1 mJy) sources positionally associated within 1.5'' with a Sloan Digital Sky Survey (SDSS) (optical, sensitive to  $r^* \sim 22.2$ ) source in 1230  $deg^2$  of sky. The matched sample represented  $\sim 30\%$  of the 108,000 FIRST sources and 0.1% of the  $2.5 \times 10^7$  SDSS sources in the studied region. SDSS spectra are available for 4300 galaxies and 1154 quasars from the matched sample and for a control sample of 140,000 galaxies and 20,000 quasars in 1030  $deg^2$  of sky (Ivezić et al., 2002).

---

<sup>7</sup>ATESP radio survey. It was made at 1.4 GHz with the Australia Telescope Compact Array.

They first positionally matched all sources from both catalogs whose positions agree to better than  $3''$ , and found 37,210 such pairs. The distribution of the distance between the SDSS and FIRST positions,  $d$ , for the 10,084 pairs from the EDR<sup>8</sup> subsample is shown in the top panel in Figure 5 of Ivezić et al. (2002). In order to test whether the distance distribution depends on optical morphology, they split the SDSS EDR<sup>9</sup> sample into 1999 optically unresolved and 8085 resolved sources. The increase in the number of matches with  $d \leq 2.5''$  was consistent with expected random associations, given the number density of FIRST and SDSS sources. Based on this histogram, they choose  $1.5''$  as the limiting distance for a match to be considered as an optical identification, and they found 29,528 matches satisfying this criterion. This cutoff was a trade-off between the completeness and contamination of the sample. For a cutoff at  $3''$  practically all true matches (estimated to be 33,800 after subtracting the estimated number of random matches) were included in the sample, but the contamination from random matches was roughly 9%. On the other hand, a cutoff at  $1''$  with a contamination of 1.5% was only 72% complete. The chosen cutoff resulted in a 85% complete sample with a contamination of 3%. The high completeness and low contamination were due to the excellent astrometric accuracy of both SDSS and FIRST. As a comparison, Magliocchetti et al. (2002) used a  $2''$  cutoff for the APM-FIRST matches, and Sadler et al. (2002) used a 10-15'' cutoff for the NVSS<sup>10</sup>-2dFGRS<sup>11</sup> matches (but noted contamination). Based on statistical considerations, the 29,528 optical identifications include  $\sim 28,684$  true associations and  $\sim 844$  random matches. The estimated completeness implies that, for the 107,654 FIRST sources, there are 33,746 SDSS counterparts, or 31% of all FIRST sources (of course, because of the completeness vs. contamination trade-off, robust identifications can be made only for 27% of FIRST sources). These identifications represent  $\sim 0.14\%$  of all SDSS sources in the analyzed region.

Sullivan et al. (2004) identified candidate optical counterparts to the radio catalogs of

---

<sup>8</sup>Early Data Release.

<sup>9</sup>SDSS Early Data Release.

<sup>10</sup>NRAO VLA sky survey.

<sup>11</sup>2dF galaxy redshift survey.

the Phoenix Deep Survey<sup>12</sup>. They found that 673/839 (79%) of the radio detections had candidate optical counterparts in the images; of these 639 (76%) were detected at  $\geq 5\sigma$  in one or more filters. Taking other band-passes individually: 569/1063 (54%) in the CTIO U-band and 53/256 (21%) in the (shallower) ESO U-band had candidate counterparts detected at  $\geq 5\sigma$  significance; 91/111 (82%) of the radio detections were detected in Ks-band at  $\geq 5\sigma$ . In total, across all the data sets 1331 radio objects were observed, with candidate optical counterparts identified for 778 (58%).

Gonzalez-Solares et al. (2005), presented the multiwavelength properties and catalogue of the 15  $\mu\text{m}$  and 1.4 GHz radio sources detected in the European Large Area ISO Survey (ELAIS<sup>13</sup>). Thus, using the optical data from the Wide Field Survey and likelihood ratio method to search for the counterparts of the 1056 and 691 sources detected at 15  $\mu\text{m}$  and 1.4 GHz, respectively, down to flux limits of  $S_{15} = 0.5$  mJy and  $S_{1.4\text{GHz}} = 0.135$  mJy, they found that  $\sim 92\%$  of the sources had an optical counterpart down to  $r' = 24$ . They found also that, all mid-infrared (IR) sources with fluxes  $S_{15} \geq 3$  mJy had an optical counterpart. The magnitude distribution of the sources showed a well-defined peak at relatively bright magnitudes  $r' \sim 18$ . About 15% of the sources were bright galactic stars; of the extra-galactic objects  $\sim 65\%$  were compatible with being normal or star-burst galaxies and  $\sim 25\%$  AGNs. Objects with mid-IR-to-optical fluxes larger than 100 were found, comprising  $\sim 20\%$  of the sample. They suggest that these sources are highly obscured luminous and ultra-luminous star-burst galaxies and AGNs.

In 2006, optical counterparts of radio sources in the GOODS<sup>14</sup> ACS field<sup>15</sup> were identified using the likelihood ratio method of Sutherland and Sanders (1992) by Afonso et al. (2006). For each radio source, the optical identification with the highest relia-

<sup>12</sup>Phoenix Deep Survey is a multiwavelength galaxy survey based on deep 1.4 GHz radio imaging

<sup>13</sup>European Large Area ISO Survey.). It was a collaborative effort between 19 European institutions that has carried out a deep wide angle survey with ISO at four wavebands (6.7 and 15  $\mu\text{m}$  using CAM camera and 90 and 175  $\mu\text{m}$  with PHOT camera) over a area of about 12 square degrees of high latitude sky.

<sup>14</sup>The Great Observatories Origins Deep Survey .

<sup>15</sup>South Advanced Camera for Surveys.



bility ( $R$ ), if above 20% was taken as the real optical counterpart; if several optical identifications had similar values for ( $R$ ), the various possibilities were considered. Identifications were inspected visually to check for special situations in which the likelihood ratio method would not apply, as in the case of nonindependent sources (either in the radio or in the optical). The identification of the X-ray counterparts was performed by searching the  $3\sigma$  radio position error region. Visual inspection was used to associate the optical and X-ray identification (Afonso et al., 2006).

Boucheffry and Cress (2006) made the optical and near infrared identifications of 514 radio sources in FIRST survey<sup>16</sup> obtained by matching objects in the NDWFS<sup>17</sup> survey, over the region  $216.1^\circ \leq \text{RA} \leq 220^\circ$ ,  $34^\circ \leq \text{DEC} \leq 36^\circ$ . They positionally matched the FIRST radio sources with the two last strips of the NDWFS catalogue which covered  $5 \text{ deg}^2$  using a searching radius of 2 arcsec. Sources observed in the K-band in the  $5 \text{ deg}^2$  of interest had a surface density,  $\rho$ , of  $1.4 \times 10^{-3} \text{ sources/arcsec}^2$ . The number of FIRST sources in the region was 514. They identified 177 sources (35%) in all 4 bands of NDWFS. In the I-band, 74% of sources were identified. They found a surprisingly large difference between the number of sources in the upper declination strip and that in the lower strip, possibly explained by the presence of large-scale structure in the  $34^\circ \leq \text{DEC} \leq 35^\circ$  strip.

The CENSORS<sup>18</sup> survey Brookes et al. (2008) matches sources in the ESO Imaging Survey to 150 sources in the NRAO VLA Sky Survey and is complete to 7.8 mJy. They found that their data were not consistent with existing models for radio source evolution and further work on modelling was required.

In order to study the radio properties of optically obscured Spitzer sources, Magliocchetti et al. (2007) cross-correlated a sub-sample of optically faint ( $R \geq 25.5$ )  $24 \mu\text{m}$  - selected galaxies observed in the Spitzer FLS with the radio catalogues in the field.

<sup>16</sup>Faint Images of the Radio Sky at Twenty-centimeters.

<sup>17</sup>The NOAO Deep Wide-Field Survey. It was a deep optical and near-infrared imaging survey that covered two 9.3 square degree fields. It was designed primarily for the study of the existence and evolution of large scale structures at redshifts  $z > 1$  as sampled by diverse populations of objects.

<sup>18</sup>The Combined EIS-NVSS Survey of Radio Sources.

Using a search radius less than  $10''$ , 70 optically faint Spitzer sources were identified in the Condon et al. catalogue, 33 in the Morganti et al. (2004) dataset, while 52 were found in the survey performed by Garn et al. (2007). After performing a number of corrections to account for multiple identifications, sources erroneously split in the original Spitzer catalogue into different components and mid-IR objects with real radio counterparts at one of the allowed ( $10''$ ) matching radius, they ended up with a sample of 96 radio-identified, optically faint, mid-IR emitting sources, 45 of which had an identification at both 1.4 GHz and 610 MHz (Magliocchetti et al., 2007).





In this chapter, I briefly describe the data and the methods used to analyse it.

### 3.1 Data

Observations of the Spitzer xFLS field by the VLA were made during two successive B configurations<sup>1</sup> session during February through to May 2001 and June through to August 2002, to produce the mosaic image (Figure 3.1) and accompanying catalog (Condon et al., 2003). The left panel of Figure 3.1 shows the image of the full VLA mosaic of the FLSv. The right panel shows sources in sub-images of the FLSv field.

The VLA survey covered  $\sim 4 \text{ deg}^2$  with a resolution of  $5''$ , to a  $1 \sigma$  depth of  $\sim 23 \mu Jy$  (Condon et al., 2003). The frequency used for these observations was 1.4 GHz and contains 3565 sources (Condon et al., 2003).

The WSRT survey (Morganti et al., 2004) was centred on  $\sim 1 \text{ sq. deg.}$  field of the xFLS field to a depth of  $\sim 8.5 \mu Jy \text{ beam}^{-1}$  with a resolution of  $14'' \times 11''$ , and it contains 1048 sources. A mosaic (Figure 3.2) of 7 pointings was chosen and the central field is centred on RA(J2000)=17:17:00.00 and DEC(J2000)=59:45:00.000 . The left panel of Figure 3.2 shows the image of the full WSRT mosaic of the FLSv. The right panel shows sources in sub-images of FLSv field. The main observations were made during the period May-June 2002, and about 16 hours was spent on each pointing (Morganti et al., 2004). Two additional 12-hours observations of the central region, were carried out in Feb 2003 (Morganti et al., 2004).

<sup>1</sup>The B configuration having a maximum antenna separation of 10 km.

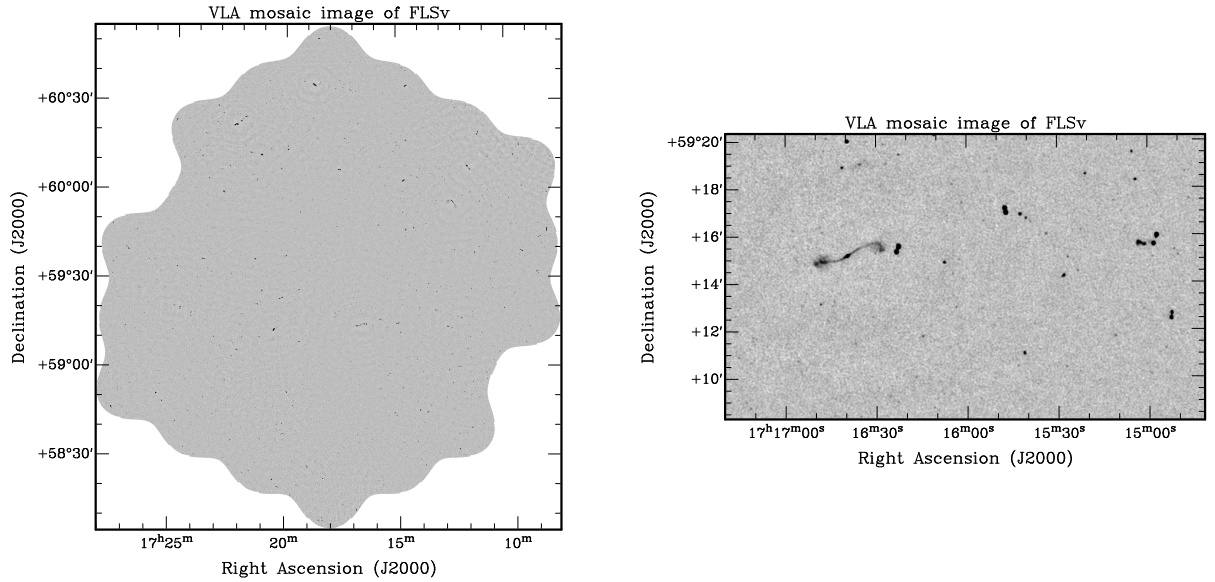


**Figure 3.1:** VLA mosaic image of FLSv.

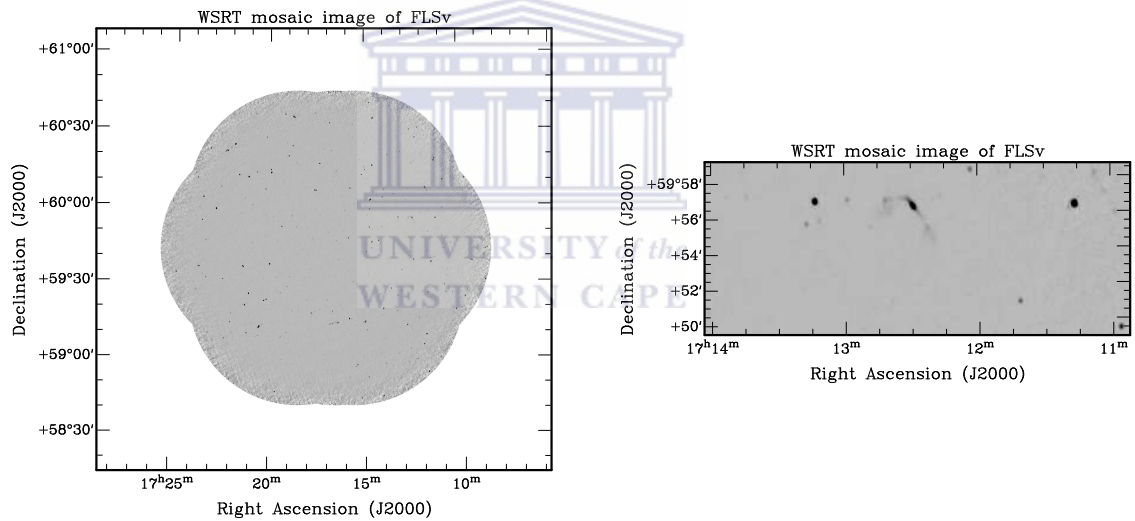


**Figure 3.2:** WSRT mosaic image of FLSv.

Observations of the Spitzer xFLS field were made at 610 GHz with the GMRT over four days in March 2004 (Garn et al., 2007). Seven pointings were observed, in a hexagonal grid centred on RA(J2000)=17:18:00.00, DEC(J2000)=59:30:00.000 as shown in Figure 3.3 (Garn et al., 2007). The left panel of Figure 3.3 shows the image of the full GMRT mosaic of the FLSv. The right panel shows sources in sub-images of FLSv field. The observation covered a total area of  $\sim 4deg^2$  with a resolution of  $5.8'' \times 4.7''$

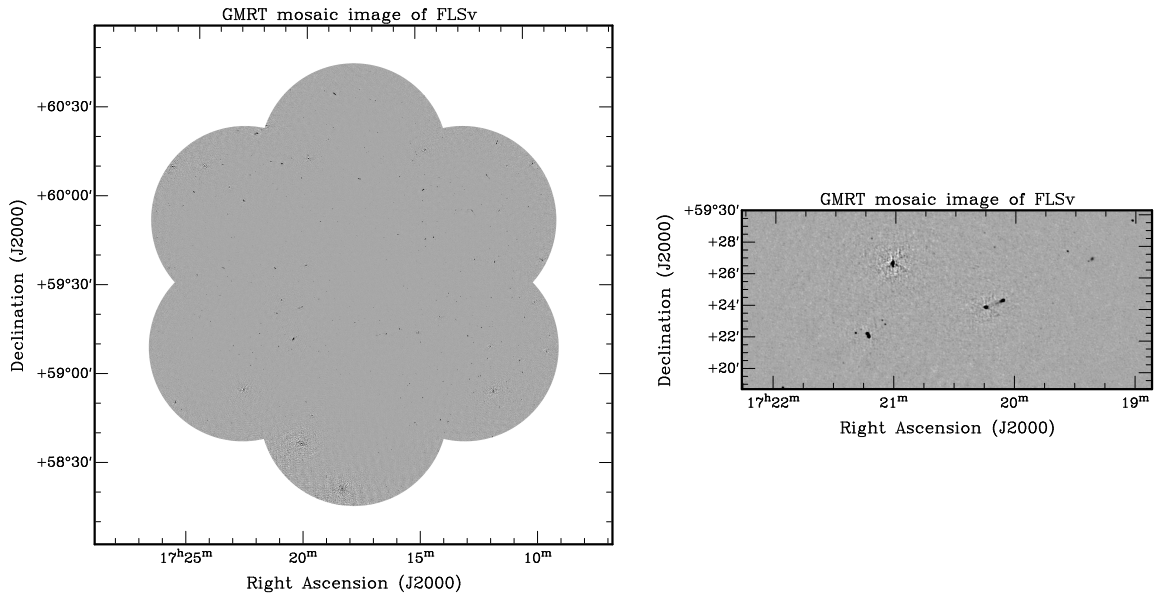


**Figure 3.3:** GMRT mosaic image of FLSv.

at positional angle (PA)  $60^\circ$  (Garn et al., 2007). The r.m.s noise at the center of the pointings was between 27 and 30  $\mu Jy$  before correction for GMRT primary beam and a total of 3944 sources were detected above  $\sim 5\sigma$  (Garn et al., 2007).

In Table 3.1, I summarize information about the area observed with respect to the sq. deg. (column 1), resolution ( $\theta$ ) in column 2, sensitivity ( $\sigma$ ) in column 3. In Column 4, I list the number of sources detected by VLA, WSRT and GMRT in the FLS field.

The redshift data used in this project, were taken from Marleau et al. (2007) and

**Table 3.1:** Area observed, resolution, sensitivity and sources detected by VLA, WSRT and GMRT in the FLS field.

	Area (deg. sq.)	$\theta$ (arcsec)	$1\sigma$ $\mu Jy/\text{beam}$	Sources
VLA	4	5	23	3565
WSRT	$\sim 1$	$14 \times 11$	8.5	1048
GMRT	$\sim 4$	$5.8 \times 4.7$	30	3944

Papovich et al. (2006) surveys of the xFLS field. Marleau et al. (2007) present an optical spectroscopic survey of 24  $\mu m$  and 1.4 GHz sources of xFLS using the multifiber

spectrograph, Hydra, on the WIYN telescope. Their WIYN/Hydra target sample was selected from two data sets of sources detected in the FLS. The first set was comprised of sources detected at 1.4 GHz and with an R-band magnitude  $< 23$ . This set was used during their 2002 and 2003 observing runs, prior to the Spitzer launch (Marleau et al., 2007). The second set was constructed from the  $24 \mu\text{m}$  sources, using the same R-band magnitude cut (Marleau et al., 2007). These were targeted during their 2005 observing run after the Spitzer observations of the FLS were completed (Marleau et al., 2007). A few companions of 1.4 GHz and  $24 \mu\text{m}$  sources were also part of the sample (Marleau et al., 2007). The same author, mentioned that the redshifts measured in the survey are mostly in the range  $0 < z < 0.4$ , with a distribution peaking at  $z \sim 0.2$ . Papovich et al. (2006), present a spectroscopy survey using the MMT/Hectospec fiber spectrograph of  $24 \mu\text{m}$  sources selected with the Spitzer Space Telescope in the Spitzer FLS. They reported 1296 new redshifts for  $24 \mu\text{m}$  sources, including 599 with  $f_\nu(24 \mu\text{m}) \geq 1 \text{ mJy}$ . Combined with 291 additional redshift for sources from SDSS, their observing program was highly efficient and is 90% complete for  $i \leq 21 \text{ mag}$  and  $f_\nu(24 \mu\text{m}) \geq 1 \text{ mJy}$ , and is 35% complete for  $i \leq 20.5 \text{ mag}$  and  $0.3 \text{ mJy} \leq f_\nu(24 \mu\text{m}) \leq 1.0 \text{ mJy}$ . Their Hectospec survey includes 1078 and 168 objects spectroscopically classified as galaxies and QSOs, respectively. Combining the Hectospec and SDSS samples, they found  $24 \mu\text{m}$  selected galaxies to  $z_{gal} \leq 0.98$  and QSOs to  $z_{QSO} \leq 3.6$ , with mean redshifts of  $z_{gal} = 0.27$  and  $z_{QSO} = 1.1$  (Papovich et al., 2006).

## 3.2 Methods

### 3.2.1 Cross-correlation of radio catalogues and spectral index derivation

Adopting the criteria based on the separation between the sources, a cross-correlation between radio sources from VLA and GMRT catalogues with positional offsets  $d < 3''$  was done with the aim of studying the radio spectral properties of the sample. After that, I extracted sub-images of multi-component sources from the VLA, GMRT and WSRT mosaic images and I visually inspected the source morphology to decide which GMRT components to sum in order to get the same source structure as for the VLA.

Using the source morphology, I also performed a preliminary classification in Fanaroff-Riley Class (FR I or FR II), Peculiar, Compact and Extended.

Using VLA and GMRT fluxes at different frequency and same spatial resolution, I measured the spectral index ( $\alpha$ , see Formula 2.9 in Chapter 2).

### 3.2.2 Optical identification

To do the optical identification, I adopt the criteria based on the separation between the sources to cross-correlate the two-frequency FLS radio catalogue with the optical catalogue of Marleau et al. (2007) and Papovich et al. (2006), assuming 6 arcsec as minimum distance.

For all multi-component sources, I had to estimate the central position using the source centroid, i.e. the flux-weighted average position of all components (Prandoni et al., 2006). For example, the centroid of two components sources was computed using the following formula:

$$ra_b = (ra_1 * w_1) + (ra_2 * w_2) \quad (3.1)$$

$$dec_b = (dec_1 * w_1) + (dec_2 * w_2) \quad (3.2)$$

Where:  $ra$  stands for right ascension and  $ra_b$  stands for the  $ra$  barycenter position.  $dec$  stands for declination and  $dec_b$  stands for  $dec$  barycenter position.  $w_1 = st_1/st_{tot}$ ,  $w_2 = st_2/st_{tot}$  and  $st_{tot} = st_1 + st_2$ , here  $st_{tot}$ ,  $w_1$ ,  $w_2$  are integrated global sources flux densities and weight's respectively.

An overlay between radio sources optically identified and deep NOAO optical images of the FLS field was done using Karma software<sup>2</sup>. As an example, I show the overlay between a radio and a shallow optical image of a small section of FLSv field obtained from Nasa Extra-galactic Database<sup>3</sup> in Figure 3.4. Figure 3.4 also shows the

<sup>2</sup><http://www.atnf.csiro.au/computing/software/karma/>

<sup>3</sup>NED - <http://nedwww.ipac.caltech.edu>

VLA mosaic image as background and a shallow optical image as a green box in the top panel. By zooming, you can see the contours indicating the presence of a galaxy at the center of the radio source (see bottom panel of the Figure 3.4).



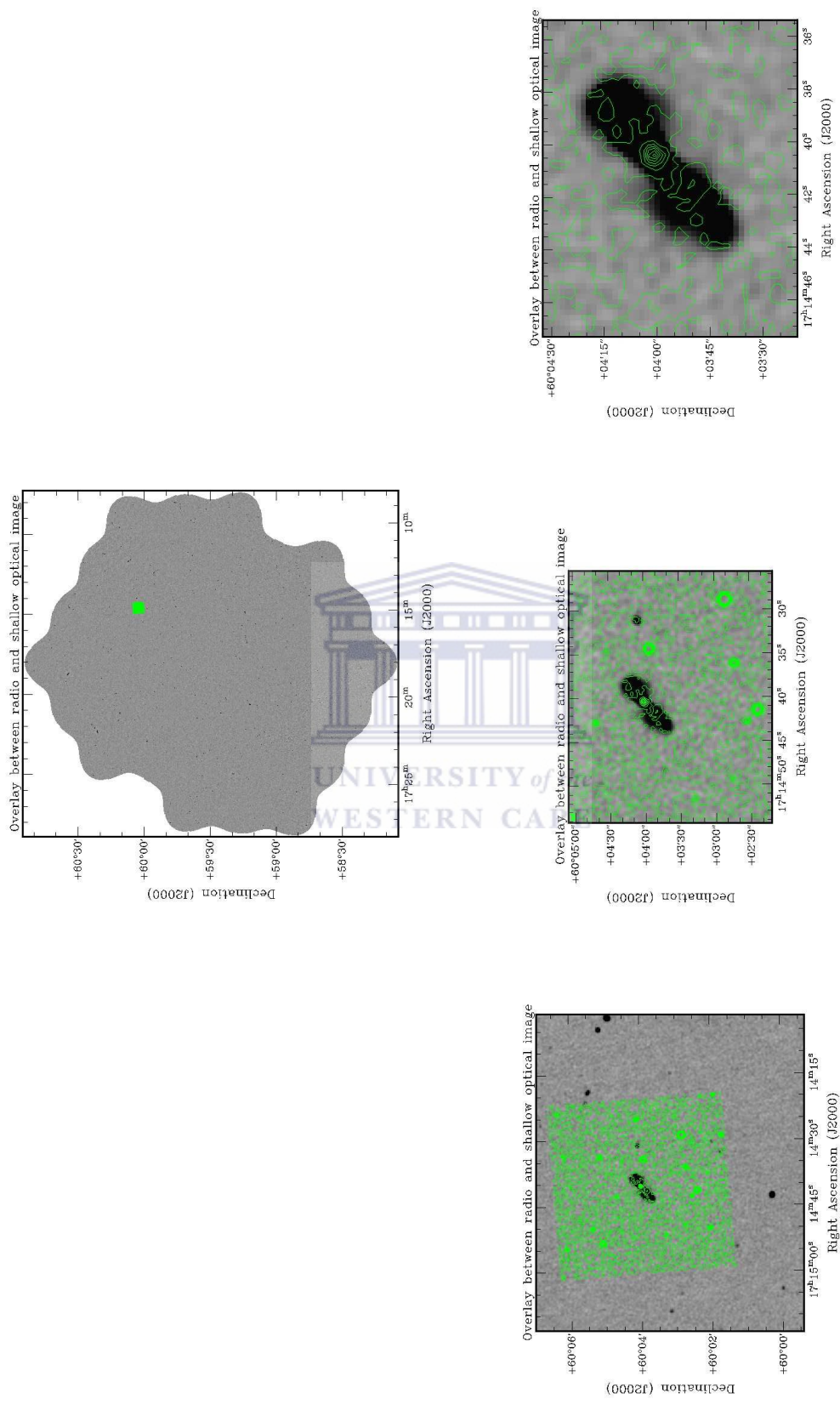


Figure 3.4: Example of overlay between radio and optical image of the FLSv field.



### 3.2.3 Derivation of radio and optical luminosity

Radio and optical luminosities of all identified sources with determined redshifts were measured using Formulas 3.3 and 3.4, respectively. In these formulas,  $L$  stands for the radio luminosity,  $d_l$  for luminosity distance,  $S$  for integrated flux,  $M$  and  $m$  for absolute and apparent magnitude.

$$L = 4\pi(d_l)^2 * S \quad (3.3)$$

$$M = m - 25 - (5 * \log_{10}(d_l)) \quad (3.4)$$

All values of luminosity distance used here, were calculated using a cosmology calculator. According to Edward (2006), the calculator computes times and distances as a function of redshift for user-defined cosmological parameters, and is available at <http://www.astro.ucla.edu/wright/CosmoCalc.html>. A cosmology of  $H_o = 71$ ,  $\Omega_M = 0.27$  and  $\Omega_{vac} = 0.73$  was assumed during this calculation.

UNIVERSITY of the  
WESTERN CAPE



---

## Results and Discussion

---

In this chapter, I present the results and the discussion of our study. I start by showing the results of the cross-correlation between radio catalogues and morphological classification of sources in the FLSv field. I then calculate and discuss the radio spectral indices. Results of the optical identification of the FLSv radio sources are shown and discussed. Finally, I show the results for the luminosity and classification of the sources optically identified in the FLSv field.

### 4.1 Cross-correlation of radio catalogues and morphological classification of sources in the FLSv

After cross-correlating the VLA and GMRT data, I obtained a catalogue of 1573 radio component sources from which a sub-sample of 201 source candidates appeared to be part of multi-component systems. Among these 201 sources, a sample of 165 multi-component sources were extracted and sub-images of them were produced.

By visual inspection of the 165 sub-images, all the components of the same source were combined in order to decide how to sum the fluxes for the GMRT components to ultimately get the same source structure as VLA. Thus, I got a sample of 107 radio sources for my study (see Section 3.2 to know how I got It), where: 58 consist of one component, 42 two components, 6 three components and one consists of four components (see Table 4.1).

I list all identified radio sources in right ascension order in Table 4.1. Column 1 and 2

gives the right ascension and declination of the sources in decimal degree, identified after cross-correlation of the VLA and GMRT catalogues. Normally, the position of the sources are either the centroids of simple double sources or the fitted positions of central components in triple and quadruple sources. Column 3 gives the International Astronomical Union (IAU) designation for the source, in the form Jhhmmss.s+ddmmss, where J represents J2000.0 coordinates, hhmmss.s represents right ascension in hours, minutes and truncated tenths of seconds, and ddmms represents the declination in degrees, arcminutes and arcseconds. Column 4 gives the information about the number of components from the sources after cross-correlation of the GMRT and VLA data. Column 5 is the Source Extractor deblended object flag which is 0 for most objects, but 1 when a source has been split up into two or more components (Garn and Alexander, 2008). Column 6 gives the VLA group label for multi-component sources. Column 7 gives the VLA number of components in the group. Column 8 gives the VLA integrated 1.4 GHz flux density (in mJy). Column 9 gives the GMRT Peak 0.61 GHz flux density. Column 10 gives the GMRT integrated 1.4 GHz flux density (in mJy). Column 11 gives spectral index.

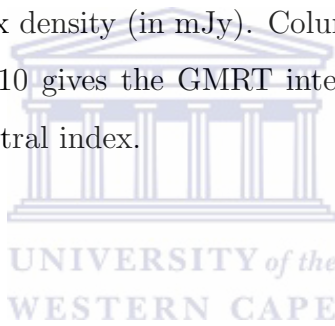


**Table 4.1:** Radio multi-component sources cross - identified between VLA and GMRT catalogues.

RA (deg.)	Dec (deg)	Name	NC cross-id	Flags	CG VLA	NC VLA	I. S (mJy) VLA	P. S (mJy) GMRT	I. S (mJy) GMRT	$\alpha$
(1)	(2)	(3)	(4)	(5)	(6)	(7)	(8)	(9)	(10)	(11)
257.338464	60.024983	J170921.2+600130	1	0	G007	4	3.89	2.46	8.14	-0.89
257.351471	59.656837	J170926.4+593935	3	0	G008	4	38.77	46.98	99.64	-1.14
257.427171	60.200678	J170942.5+601202	1	0	G009	2	28.07	33.26	80.72	-1.27
257.473541	59.811325	J170952.5+594847	2	0	G010	4	1.79	0.80	3.07	-0.65
257.484923	59.958900	J170956.4+595732	1	0	G011	2	3.90	2.98	10.75	-1.22
257.566677	59.338456	J171016.0+592018	1	0	G012	2	14.89	9.14	27.49	-0.74
257.638050	59.601789	J171033.1+593606	1	0	G013	2	1.61	0.91	1.19	0.36
257.684881	59.915678	J171044.4+595456	1	0	G014	2	1.60	1.06	1.53	0.05
257.734758	59.711456	J171056.4+594241	1	1		1	0.48	0.31	0.73	-0.50
257.771637	59.963856	J171105.2+595751	4	0	G015	6	3.16	0.79	4.55	-0.44
257.816923	59.941983	J171116.1+595631	1	0	G016	2	28.77	47.91	57.63	-0.84
257.824524	60.324146	J171116.3+601958	2	0	G017	2	41.95	22.32	108.48	-1.14
257.826385	59.203747	J171118.8+591222	2	0	G018	3	2.23	2.62	7.41	-1.45
257.882507	59.654751	J171131.8+593924	2	1	G019	2	26.33	39.31	90.19	-1.48
257.890342	59.521511	J171133.7+593117	1	1		1	0.15	0.28	0.34	-0.95
257.946564	60.141495	J171145.4+600808	2	0	G020	7	23.64	5.80	26.04	-0.12
258.027222	58.870817	J171206.5+585215	1	0	G022	2	1.92	1.21	3.36	-0.67
258.052856	59.288933	J171213.8+591723	3	0	G023	5	6.56	2.61	16.49	-1.11
258.072968	59.014122	J171215.4+590053	2	0	G024	2	9.21	6.26	22.87	-1.09
258.127014	59.944828	J171229.1+595639	3	0	G026	13	31.57	7.43	35.35	-0.14
258.140386	59.305733	J171233.7+591820	1	1		1	0.18	0.44	0.59	-1.40
258.157762	59.084956	J171237.9+590506	1	0	G027	2	3.32	2.07	6.94	-0.89
258.164306	58.696233	J171239.4+584146	1	0	G028	2	1.49	1.39	3.79	-1.12
258.187775	58.996674	J171245.3+585942	2	1	G029	2	4.80	2.10	8.47	-0.68
258.197928	59.241122	J171247.5+591428	1	0	G030	3	12.86	7.44	27.91	-0.93
258.325500	59.332455	J171319.4+592000	2	0	G031	5	5.38	2.75	6.99	-0.32
258.348258	59.607650	J171323.6+593627	1	1		1	0.63	0.94	1.10	-0.67
258.420299	59.822206	J171340.9+594920	1	0	G032	2	0.86	0.69	2.40	-1.24
258.429382	58.760315	J171344.4+584533	2	1	G033	3	6.91	2.47	13.74	-0.83
258.448796	60.106428	J171347.7+600623	1	1		1	0.15	0.28	0.45	-1.34

Table 4.2: Continuation of Table 4.1.

RA (deg.)	Dec (deg)	Name	NC cross-id	Flags	CG VLA	NC VLA	I. S (mJy) VLA	P. S (mJy) GMRT	I. S (mJy) GMRT	$\alpha$
(1)	(2)	(3)	(4)	(5)	(6)	(7)	(8)	(9)	(10)	(11)
258.457047	59.979317	J171349.7+595845	1	1		1	0.13	0.29	0.33	-1.16
258.511383	58.772739	J171403.1+584609	2	1	G035	2	19.82	13.58	44.40	-0.97
258.539221	59.069539	J171409.4+590410	1	1		1	0.71	0.60	1.16	-0.59
258.558960	59.798855	J171414.6+594750	2	1	G036	2	15.90	11.65	41.23	-1.15
258.638298	59.878150	J171433.2+595241	1	1		1	0.16	0.34	0.39	-1.09
258.649292	59.789276	J171437.0+594711	2	1	G038	2	11.74	5.56	25.28	-0.92
258.667630	60.067011	J171440.2+600401	1	0	G039	3	30.31	7.60	57.54	-0.77
258.680389	59.886490	J171442.9+595309	2	1		1	8.29	11.12	17.78	-0.92
258.691224	58.588983	J171445.9+583520	1	0	G040	2	1.22	1.10	3.44	-1.25
258.699055	58.897372	J171447.8+585350	1	0	G041	2	8.26	8.01	19.48	-1.03
258.717102	59.209885	J171452.2+591231	2	1	G042	2	3.73	2.85	8.22	-0.95
258.741211	59.264473	J171457.9+591539	3	0	G043	5	25.02	26.38	63.18	-1.12
258.776056	58.713567	J171506.3+584249	1	1		1	0.25	0.51	0.60	-1.08
258.787514	58.757261	J171509.0+584526	1	0	G044	2	10.11	8.42	24.44	-1.06
258.945557	59.285107	J171546.8+591702	2	1	G045	2	17.53	14.22	41.90	-1.05
259.094635	59.258568	J171622.4+591536	2	1	G046	2	14.75	8.65	33.54	-0.99
259.114670	60.343067	J171627.5+602035	1	1		1	0.12	0.32	0.31	-1.12
259.178040	59.251705	J171639.4+591513	3	1	G047	9	19.65	2.98	12.99	0.50
259.178753	60.390122	J171642.9+602324	1	0	G048	2	2.79	3.68	7.17	-1.14
259.263214	60.577461	J171702.0+603434	2	0	G050	3	3.61	1.29	6.22	-0.65
259.331299	60.304821	J171719.6+601817	2	0	G051	2	18.28	15.21	16.86	0.10
259.353630	60.117428	J171724.9+600703	1	1		1	0.18	0.31	0.36	-0.85
259.355584	60.592067	J171725.4+603531	1	1		1	1.43	0.32	0.38	1.60
259.388855	60.130226	J171735.9+600752	2	1	G052	4	20.99	7.33	44.99	-0.92
259.417206	59.809586	J171741.2+594836	2	1		1	1.08	0.80	3.28	-1.34
259.440582	59.301025	J171744.1+591817	2	0	G053	2	2.42	0.44	1.58	0.51
259.474674	59.716733	J171753.9+594300	1	1		1	0.38	0.52	2.01	-2.00
259.482380	60.088622	J171755.8+600519	1	1		1	0.14	0.19	0.26	-0.79
259.591090	59.783011	J171821.9+594659	1	0	G054	3	0.64	0.27	1.36	-0.91
259.669800	60.608719	J171841.3+603630	2	0	G058	8	43.80	5.30	69.93	-0.56

Table 4.3: Continuation of Table 4.1.

RA (deg.)	Dec (deg)	Name	NC cross-id	Flags	CG VLA	NC VLA	I. S (mJy) VLA	P. S (mJy) GMRT	I. S (mJy) GMRT	$\alpha$
(1)	(2)	(3)	(4)	(5)	(6)	(7)	(8)	(9)	(10)	(11)
259.628212	60.313372	J171830.8+601848	1	0	G057	5	2.31	0.34	0.72	1.40
259.745683	58.459206	J171859.0+582733	1	0	G059	2	3.77	0.19	7.46	-0.82
259.757538	59.144878	J171902.6+590844	2	1		1	0.16	0.35	1.05	-2.24
259.825462	60.229289	J171918.1+601345	1	1		1	0.20	0.47	0.70	-1.53
259.838470	59.160835	J171922.0+590936	2	1	G060	2	4.59	1.56	6.52	-0.42
259.839050	59.453503	J171921.1+592714	2	1		1	3.03	1.33	6.65	-0.95
259.864532	59.986221	J171928.1+595906	2	0	G061	3	1.16	0.42	1.83	-0.55
259.881892	58.374789	J171931.7+582229	1	1		1	1.17	1.39	1.60	-0.37
259.968087	60.243011	J171952.4+601435	1	0	G063	3	103.53	91.50	234.36	-0.98
259.973419	58.874149	J171953.2+585222	2	1	G064	3	6.44	2.88	10.53	-0.59
259.984100	59.643391	J171956.7+593834	2	1	G065	2	42.81	41.89	106.88	-1.10
259.988181	58.761983	J171957.2+584543	1	1		1	0.33	0.41	1.11	-1.45
260.045990	59.404598	J172014.0+592407	2	0	G067	5	35.24	39.78	94.28	-1.18
260.041421	60.134011	J172009.9+600802	1	0	G068	3	8.51	3.89	16.34	-0.79
260.074843	59.444650	J172018.0+592640	1	1		1	0.30	0.35	0.46	-0.52
260.116386	59.228594	J172027.9+591343	1	0	G070	3	85.56	39.02	232.76	-1.20
260.224918	60.499594	J172054.0+602958	1	0	G072	2	1.04	0.86	1.75	-0.63
260.319489	60.218384	J172103.9+601247	2	0	G073	10	57.35	25.32	111.83	-0.80
260.301636	59.371227	J172112.1+592212	2	1	G074	2	23.74	18.00	57.67	-1.07
260.317383	60.071106	J172116.7+600406	2	0	G075	3	4.22	1.19	4.44	-0.06
260.329987	59.625679	J172119.9+593737	2	1	G076	2	38.18	27.52	97.92	-1.13
260.364380	60.099842	J172126.5+600557	2	1	G077	3	1.94	1.26	4.11	-0.90
260.446294	60.426233	J172147.1+602534	1	1	G080	3	65.87	47.88	91.65	-0.40
260.448670	60.263511	J172147.7+601548	1	0	G079	2	0.64	0.57	1.47	-1.00
260.451345	59.154094	J172148.3+590915	1	1		1	0.18	0.22	0.27	-0.48
260.490303	59.256067	J172157.7+591522	1	0	G081	2	8.88	12.05	20.75	-1.02
260.500961	60.400483	J172200.2+602401	1	0	G082	3	6.73	0.80	7.73	-0.17
260.518311	59.061188	J172204.7+590342	2	1		1	0.17	0.37	0.37	-0.92
260.558594	60.381401	J172212.5+602257	2	1	G084	4	48.53	5.96	84.66	-0.67
260.567993	58.949677	J172216.3+585701	2	1	G085	2	0.79	1.01	3.94	-1.93

**Table 4.4:** Continuation of Table 4.1.

RA (deg.)	Dec (deg)	Name	NC cross-id	Flags	CG VLA	NC VLA	I. <i>S</i> (mJy) VLA	P. <i>S</i> (mJy) GMRT	I. <i>S</i> (mJy) GMRT	$\alpha$
(1)	(2)	(3)	(4)	(5)	(6)	(7)	(8)	(9)	(10)	(11)
260.581762	59.076483	J172219.6+590435	1	0	G086	2	5.55	6.79	10.61	-0.78
260.655556	58.806650	J172237.3+584824	1	1		1	0.33	0.63	0.70	-0.89
260.690381	60.001428	J172245.7+600005	1	0	G087	2	93.14	71.39	199.36	-0.92
260.702632	59.747928	J172248.6+594452	1	1		1	0.16	0.19	0.19	-0.25
260.787964	59.797283	J172309.0+594741	2	1		1	0.76	0.76	3.39	-1.79
260.848928	59.212067	J172323.8+591243	1	1		1	0.15	0.30	0.41	-1.24
260.888885	60.257778	J172332.0+601527	2	0	G091	3	3.11	1.47	3.61	-0.18
260.898102	60.331005	J172337.1+602000	2	0	G093	4	4.37	0.59	3.56	0.25
260.904785	59.621223	J172336.4+593715	2	1	G094	4	23.68	19.85	42.31	-0.70
261.019640	58.724567	J172404.7+584328	1	1		1	0.29	0.66	0.74	-1.13
261.032715	59.317177	J172407.8+591905	2	0	G095	5	9.36	1.99	7.38	0.29
261.153809	59.343521	J172437.3+592017	3	0	G097	7	6.84	0.73	8.35	-0.24
261.227803	59.223678	J172454.7+591325	1	0	G099	2	2.44	1.67	4.39	-0.71
261.455924	59.795428	J172549.4+594743	1	1		1	0.18	0.47	0.73	-1.72
261.471845	59.093150	J172553.2+590535	1	0	G101	2	1.16	0.54	1.51	-0.32
261.503471	58.944928	J172600.8+585641	1	1		1	0.44	0.86	1.12	-1.13
261.637136	59.223844	J172632.9+591326	1	1		1	0.40	0.72	1.16	-1.28

I performed a preliminary classification of the radio source morphology into Fanaroff and Riley Class I/II (Fanaroff and Riley, 1974), Peculiar, Compact, Extended, etc. I show some examples of different morphologies in Figures 4.1 and 4.2.

The source located in the left panel of Figure 4.1 has a morphology of Fanaroff and Riley Class I (FR I). They are lower power objects showing a variety of forms in which the highest brightness occurs near their centers, excluding their cores, thus they are edge-darkened (Snellen and Best, 2001). The grey scale is from the VLA data. The red contour is the GMRT data and the levels are: 3, 4.5, 6, 10, 20, 50  $\mu Jy/beam$ . The Cyan contour is WSRT and the levels are: 6, 10, 20, 50  $\mu Jy/beam$ . The right panel of the Figure, shows a source having the morphology of Fanaroff and Riley Class II. They are more powerful sources having their regions of highest surface brightness at the ends of a double-lobed structure, thus they are edge-brightened (Snellen and Best, 2001). The grey scale and contours are the same as in the FRI image. The source

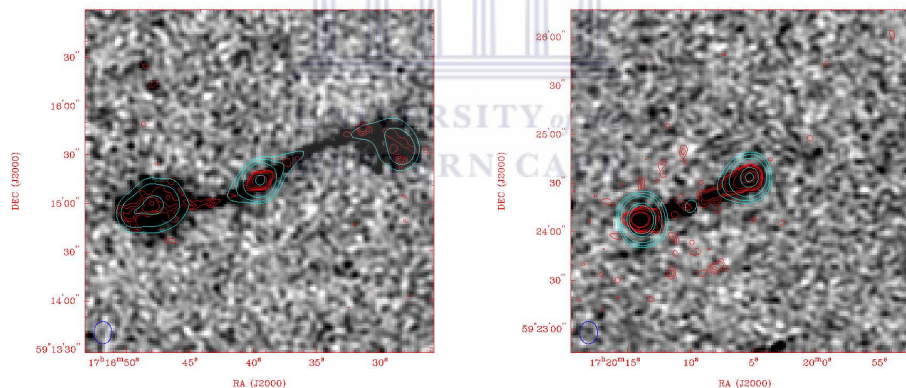


**Figure 4.1:** Example of preliminary classification of the radio source morphology: Fanaroff and Riley Class I/II.

in the Figure 4.2 shows a low surface brightness wide angle tail (WAT) source, i.e., a radio source located in cluster of galaxies (Owen and Rudnick, 1976). The grey scale and contours are the same as in the FR I image. The WSRT contours are unreliable because this source is located on the edge of the WSRT mosaic image.



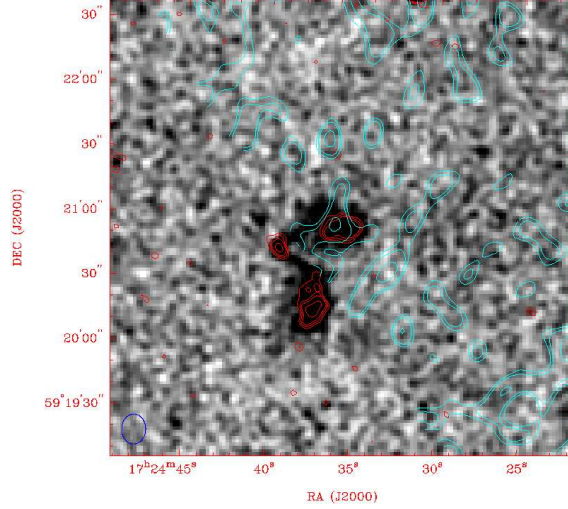


**Figure 4.2:** Example of preliminary classification of the radio source morphology: WAT.

## 4.2 The radio spectral index

Values of the radio spectral index for the sources in our sample are given in column 11 of Table 4.1. Figure 4.3 shows the radio spectral index as a function of flux density for the VLA in the left panel. The right panel shows the spectral index distribution for the same sources as shown on the left and the vertical dashed line indicates the average spectral index value of our sample ( $\alpha = -0.80$ ). As expected, the majority

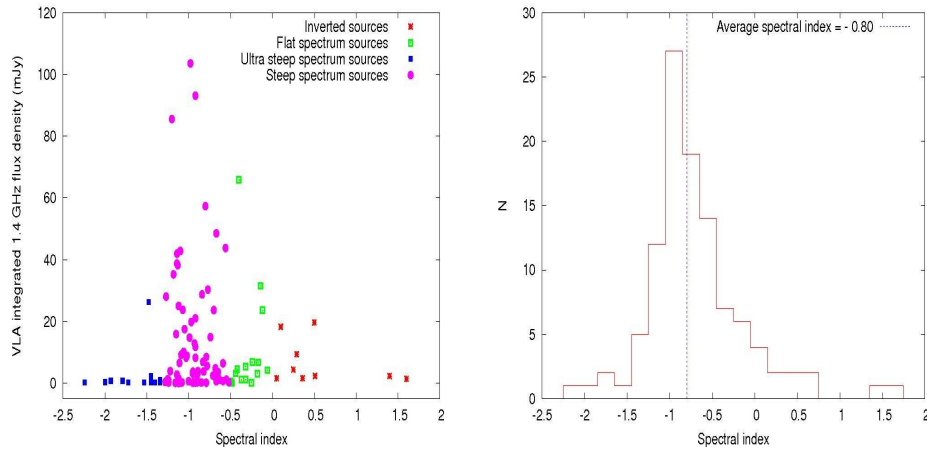


**Figure 4.3:** Spectral index.

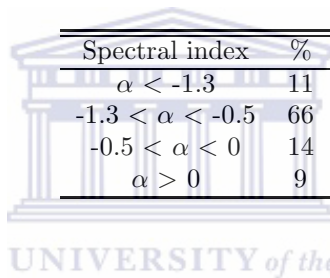
of multi-component sources are step-spectrum sources (see Figure 4.3 and Table 4.5 for statistical information). Nevertheless, the spread in the spectral distribution is



wide, with a significant number of ultra, flat or inverted sources in agreement with Prandoni et al. (2006). This indicates the presence of an heterogeneous population, consisting of a mixture of flat/steep-spectrum AGNs and steep star-forming galaxies (Prandoni et al., 2006). On the other hand, the ultra-steep spectrum sources ( $\alpha < -1.3$ ) present in the sample, if real, could potentially be associated with high redshift galaxies (Prandoni et al., 2006).

In Table 4.5, I list the statistical information on spectral index properties for multi-component sources. In Column 1, I list intervals for spectral index and Column 2 the name attributed per interval. In Column 2, I list the information about the percentage of sources per interval. Note that multi-frequency radio observations are important

**Table 4.5:** Statistical information on spectral index ( $\alpha$ ) properties for multi-component sources in the FLSv field.



Spectral index	%
$\alpha < -1.3$	11
$-1.3 < \alpha < -0.5$	66
$-0.5 < \alpha < 0$	14
$\alpha > 0$	9

because radio spectral indices may help to constrain the origin of the radio emission in the faint radio sources and may actually be fundamental for understanding eventual links to the optical light (Mignano et al., 2008).

### 4.3 Optical identification of the FLSv radio sources

The cross-correlation between 107 multi-component radio sources (see Table 4.1) with the Marleau et al. (2007) and Papovich et al. (2006) catalogues gave us 26 identifications. Among them, 15 sources have been identified by Marleau et al. (2007) and 11 sources by Papovich et al. (2006) (see Table 4.6). I list all optically identified sources ordered by right ascension, in Table 4.6. I list the right ascension and declination of the sources in decimal degree in Column 1 and 2. In Column 3, I list the IAU designation of the source, in the form Jhhmmss.s+ddmmss, where J represents J2000.0 coordinates, hhmmss.s represents right ascension in hours, minutes and truncated tenths of seconds,

and ddmss represents the declination in degrees, arcminutes and arcseconds. The \*, \*\* and \*\*\* symbols, represents sources having the same position and identified both in Marleau et al. (2007) and Papovich et al. (2006) catalogues. In Column 4, I list the VLA integrated 1.4 GHz flux density (in mJy). Column 5 lists the GMRT integrated 1.4 GHz flux density (in mJy). Column 6 lists the spectral index. Column 7 lists the redshift. Columns 8 and 9 lists the information about optical counterpart apparent magnitude and band respectively. Column 10 lists the information about identification source. Column 11 lists the information about sources with redshift from NED.



**Table 4.6:** Optical identified multi-component sources of FLSv.

RA	Dec	Name	I. S VLA (mJy)	I. S GMRT (mJy)	$\alpha$	z	mag	band	Identification Source	Sources having z from NED
(deg)	(deg)	(3)	(4)	(5)	(6)	(7)	(8)	(9)	(10)	(11)
257.637737	59.601894	J171033.1+593606	1.61	1.19	0.36	0.77890	20.5	R	Marleau et al. (2007)	NED
257.684783	59.915758	J171044.4+595456	1.60	1.53	0.05	0.22346	18.7	R	Marleau et al. (2007)	NED
258.348292	59.607806	J171323.6+593627*	0.63	1.10	-0.67	0.17550	18.3	R	Marleau et al. (2007)	
258.418671	59.821358	J171340.9+594920	0.86	2.40	-1.24	1.78200	22.8	R	Marleau et al. (2007)	NED
258.539042	59.070028	J171409.4+590410	0.71	1.16	-0.59	0.15492	19.0	R	Marleau et al. (2007)	NED
259.474700	59.716650	J171753.9+594300	0.38	2.01	-2.00	0.20650	19.3	g	Marleau et al. (2007)	
259.591300	59.782989	J171821.9+594659	0.64	1.36	-0.91	0.30500	19.2	R	Marleau et al. (2007)	
259.864217	59.985828	J171928.1+595906	1.16	1.83	-0.55	0.09582	17.2	g	Marleau et al. (2007)	NED
260.041021	60.133950	J172009.9+600802	8.51	16.34	-0.79	0.70640	20.9	R	Marleau et al. (2007)	NED
260.073500	59.444669	J172018.0+592640	0.30	0.46	-0.52	0.30541	19.9	R	Marleau et al. (2007)	
260.118000	59.228269	J172027.9+591343	85.56	232.76	-1.20	0.22090	19.1	g	Marleau et al. (2007)	
260.581571	59.076467	J172219.6+590435**	5.55	10.61	-0.78	0.03020	15.7	g	Marleau et al. (2007)	
260.702392	59.747903	J172248.6+594452	0.16	0.19	-0.25	0.17696	18.6	R	Marleau et al. (2007)	NED
261.227450	59.223633	J172454.7+591325	2.44	4.39	-0.71	0.06638	18.6	R	Marleau et al. (2007)	NED
261.637725	59.223764	J172632.9+591326***	0.40	1.16	-1.28	0.14150	17.5	R	Marleau et al. (2007)	
258.165200	58.696740	J171239.4+584146	1.49	3.79	-1.12	0.16535	18.2	g	Papovich et al. (2006)	
258.668700	60.066760	J171440.2+600401	30.31	57.54	-0.77	0.21493	18.7	g	Papovich et al. (2006)	
260.581700	59.076490	J172219.6+590435**	5.55	10.61	-0.78	0.03005	15.7	g	Papovich et al. (2006)	
257.890660	59.521990	J171133.7+593117	0.15	0.34	-0.95	0.50175	20.9	R	Papovich et al. (2006)	
258.348300	59.607790	J171323.6+593627*	0.63	1.10	-0.67	0.17508	18.3	R	Papovich et al. (2006)	
260.446960	60.263670	J172147.7+601548	0.64	1.47	-1.00	0.36084	20.3	R	Papovich et al. (2006)	
260.489260	59.256100	J172157.7+591522	8.88	20.75	-1.02	0.53926	20.0	R	Papovich et al. (2006)	
260.570220	58.948480	J172216.3+585701	0.79	3.94	-1.93	0.38601	19.6	R	Papovich et al. (2006)	
260.655610	58.806660	J172237.3+584824	0.33	0.70	-0.89	0.31417	19.4	R	Papovich et al. (2006)	
261.019960	58.724590	J172404.7+584328	0.29	0.74	-1.13	0.23902	19.2	R	Papovich et al. (2006)	
261.637790	59.223770	J172632.9+591326***	0.40	1.16	-1.28	0.14132	17.5	R	Papovich et al. (2006)	

From Figure 4.4, which shows the position (RA and DEC in degrees) in the sky of optically identified multi-component radio sources, you can see that 3 sources were identified in both the Marleau et al. (2007) and Papovich et al. (2006) catalogues (see column 3 of Table 4.6). Thus, I have a sample of 23 optical identified sources having

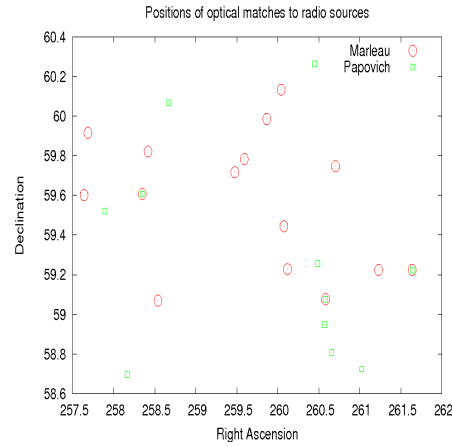


**Figure 4.4:** Positions of optical identified sources in the FLSv.

redshifts measured. Among them, redshifts of 18 sources come from the Marleau et al. (2007) and Papovich et al. (2006) catalogues. To recover the missing redshifts I used NED (see column 11 of Table 4.6). In Figure 4.5, you can see the redshift distribution of all sources, which span the range  $0 < z < 1.8$  and peaks at  $z \sim 0.2$ .

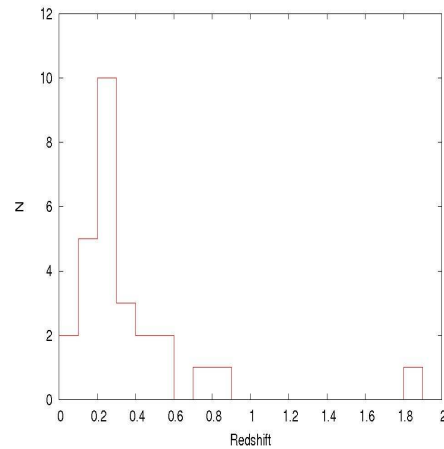


**Figure 4.5:** Redshift distribution of sources optical identified in the FLSv field.

## 4.4 Luminosity and classification of sources optical identified in the FLSv

For sources with redshifts, I computed the radio and optical luminosities (see Figure 4.7). I also performed the morphological and spectroscopic classification of all optically identified sources in the FLSv (see Table 4.7). In column 1 of Table 4.7, I list the source name, and column 2 lists the luminosity distance in Mpc. In column 3 and 4, I list the radio luminosity and radio power for VLA at 1.4 GHz respectively. Radio luminosity and radio power for the GMRT at 0.61 GHz are listed in column 5 and 6, respectively. In column 7, I list the optical luminosity, and in column 8, I list the morphological classification made by visually inspecting all sources optically identified in the FLSv. In Column 9, I list the available spectroscopic sub-classification according to Marleau et al. (2007), Papovich et al. (2006) and NED. Note that a, b, e, Sbrst and Sfom means absorption, break, emission, star-burst and star-forming, respectively.



**Table 4.7:** Information about: radio luminosity, optical luminosity and classification of sources optical identified in the FLSv.

Name (1)	DI (Mpc) (2)	L VLA (3)	Radio Power VLA (4)	L GMRT (5)	Radio Power GMRT (6)	Optical Luminosity (7)	Morphological Classification (8)	Spectroscopic Subclass (9)
J171033.1+593606	4730	4.31E+024	24.63	3.19E+024	24.50	-22.87	Extended (VLA) and Compact (GMRT)	Sbrst
J171044.4+595456	1070	2.19E+023	23.34	2.10E+023	23.32	-21.45	FRI	
J171340.9+594920	13275	1.81E+025	25.26	5.06E+025	25.70	-22.82	FR II	
J171409.4+590410	711	4.29E+022	22.63	7.02E+022	22.85	-20.26	FRI	
J171753.9+594300	978	4.35E+022	22.64	2.30E+023	23.36	-20.65	Extended	3a
J171821.9+594659	1528	1.79E+023	23.25	3.80E+023	23.58	-21.72	FRI	1e4a
J171928.1+595906	422	2.47E+022	22.39	3.90E+022	22.59	-20.93	FRI	
J172009.9+600802	4191	1.79E+025	25.25	3.43E+025	25.54	-22.21	FR II	b
J172018.0+592640	1530	8.40E+022	22.92	1.29E+023	23.11	-21.02	Compact	6a
J172027.9+591343	1057	1.14E+025	25.06	3.11E+025	25.49	-21.02	FR II	
J172219.6+590435	126	1.05E+022	22.02	2.02E+022	22.30	-19.80	FRI	7e/Sfom
J172248.6+594452	823	1.30E+022	22.11	1.54E+022	22.19	-20.98	Compact	
J172454.7+591325	286	2.39E+022	22.38	4.30E+022	22.63	-18.68	FRI	
J171239.4+584146	764	1.04E+023	23.02	2.65E+023	23.42	-21.22	Peculiar	Sbrst
J171440.2+600401	1024	3.80E+024	24.58	7.22E+024	24.86	-21.35	FRI	
J171133.7+593117	5533	5.49E+023	23.74	1.25E+024	24.10	-22.81	Compact	
J171323.6+593627	814	4.99E+022	22.70	8.72E+022	22.94	-21.25	Compact	6e2a
J172147.7+601548	1860	2.65E+023	23.42	6.08E+023	23.78	-21.05	Compact	
J172157.7+591522	3010	9.63E+024	24.98	2.25E+025	25.35	-22.39	FRI	
J172216.3+585701	2014	3.83E+023	23.58	1.91E+024	24.28	-21.92	Compact	
J172237.3+584824	1582	9.88E+022	22.99	2.10E+023	23.32	-21.60	Compact	
J172404.7+584328	1154	4.62E+022	22.66	1.18E+023	23.07	-21.11	Compact	Sfom
J172632.9+591326	642	1.97E+022	22.30	5.72E+022	22.76	-21.54	Compact	4e/Sfom

Identifying the optical counterparts of the sources is crucial in getting information on both the galaxy redshift and classification (broad/narrow-line AGN, star-forming or early type galaxy) (Prandoni et al., 2009). My results show that all identified objects are spectroscopically classified as galaxies. Some of them are classified as star-forming or star-burst galaxies, perhaps indicating that AGN and star-formation activity are ongoing in the same galaxy.

According to their radio power ( $P$ ) (see Figure 4.6), 6 of the identified objects are in the range of FR II sources ( $P_{1.4GHz} > 10^{24.5}W/Hz$ ) while 17 are in the range of FR I sources ( $P_{1.4GHz} < 10^{24.5}W/Hz$ ). Note that the horizontal line in the Figure is the division ( $P_{1.4GHz} = 10^{24.5}W/Hz$ ) between the two classes. Putting together

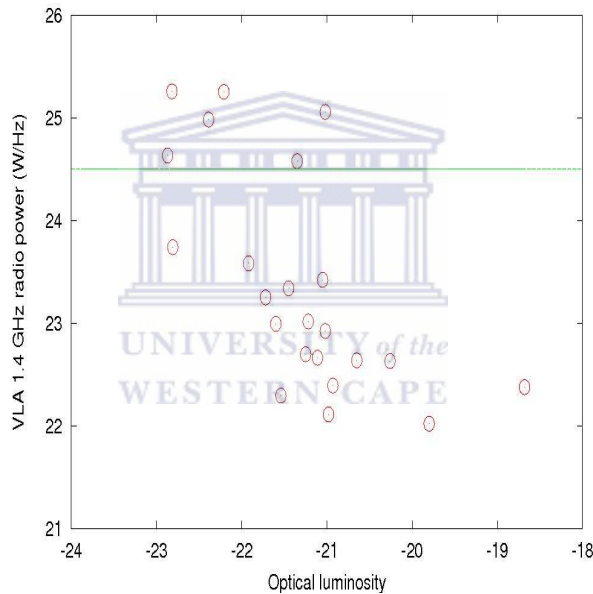


**Figure 4.6:** Optical luminosity versus radio power of sources optical identified in the FLSv.

radio images of all identified sources in order of radio power, I found that most of sources having  $P_{1.4GHz} < 10^{24.5}W/Hz$  are compact and few are extended and peculiar (see Figures 4.7 to 4.9), while all sources in the range of  $P_{1.4GHz} > 10^{24.5}W/Hz$  are extended (see Figure 4.10).

The morphology of all identified sources, are shown from Figure 4.7 to 4.10. The gray scale is the VLA data and the red contour is the GMRT data where the levels are: 3, 4.5, 6, 10, 20, 50  $\mu Jy/beam$ . The Cyan contour is WSRT and the levels are: 6,

10, 20, 50  $\mu Jy/beam$ . Table 4.8 lists the source name of all images from Figure 4.7 to 4.10 in which the corresponding morphological classification are shown in Table 4.7.





**Table 4.8:** Source name of the images in Figures 4.7, 4.8, 4.9 and 4.10.

	Figure 4.7	Figure 4.8
row 1	J172219.6+590435 & J172248.6+594452	J171753.9+594300 & J172404.7+584328
row 2	J172632.9+591326 & J172454.7+591325	J171323.6+593627 & J172018.0+592640
row 3	J171928.1+595906 & J171409.4+590410	J172237.3+584824 & J171239.4+584146
	Figure 4.9	Figure 4.10
row1	J171821.9+594659, J171044.4+595456 & J172147.7+601548	J171440.2+600401 & J171033.1+593606
row2	J172216.3+585701 & J171133.7+593117	J172157.7+591522 & J172027.9+591343
row3		J172009.9+600802 & J171340.9+594920



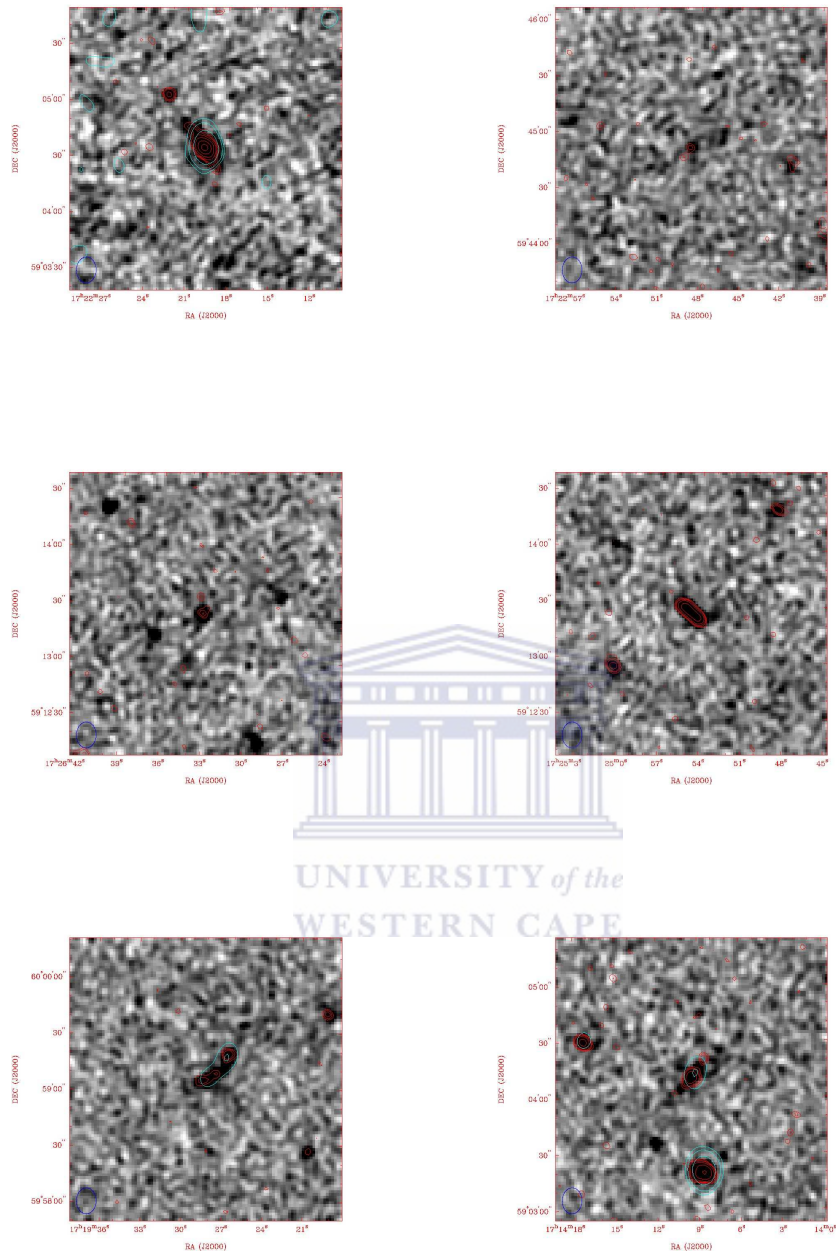


**Figure 4.7:** Radio images of sources having  $P_{1.4GHz} < 10^{24.5} W/Hz$ .

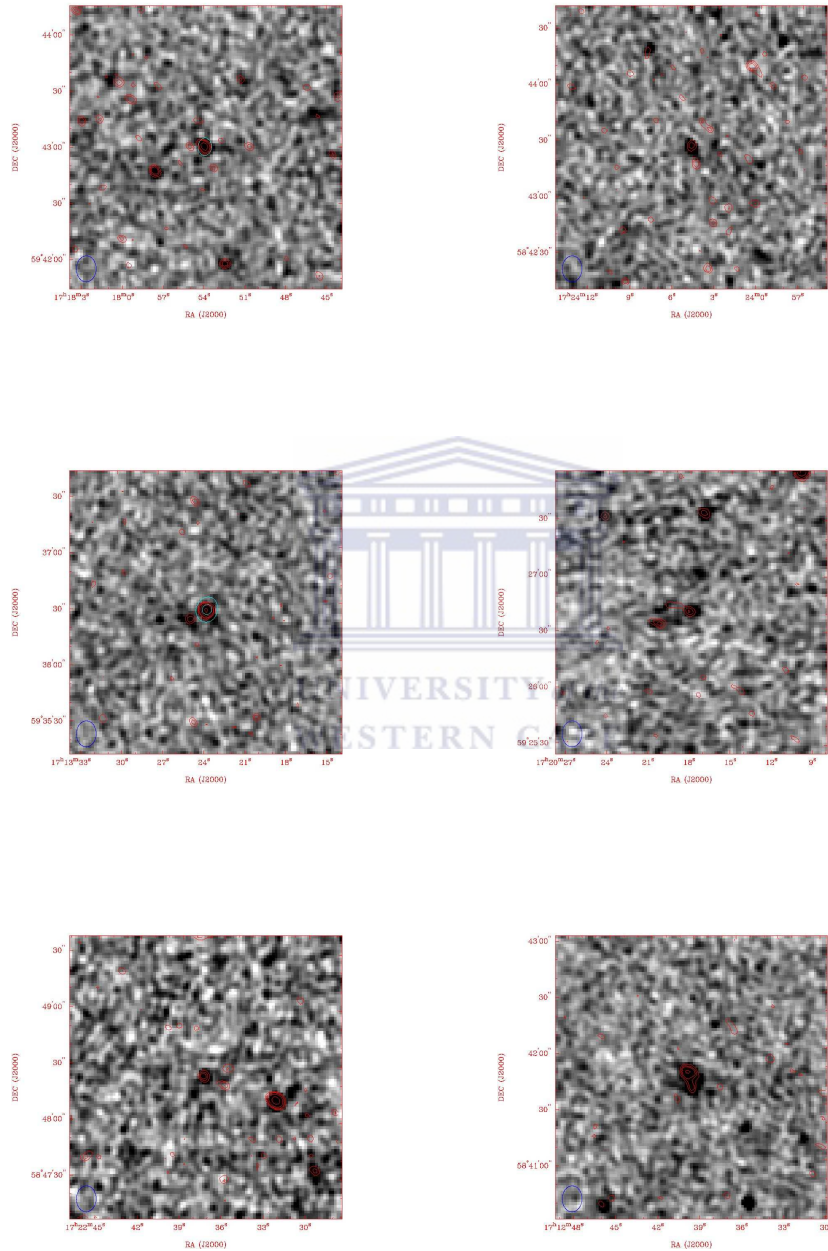


Figure 4.8: Continuation of Figure 4.7.

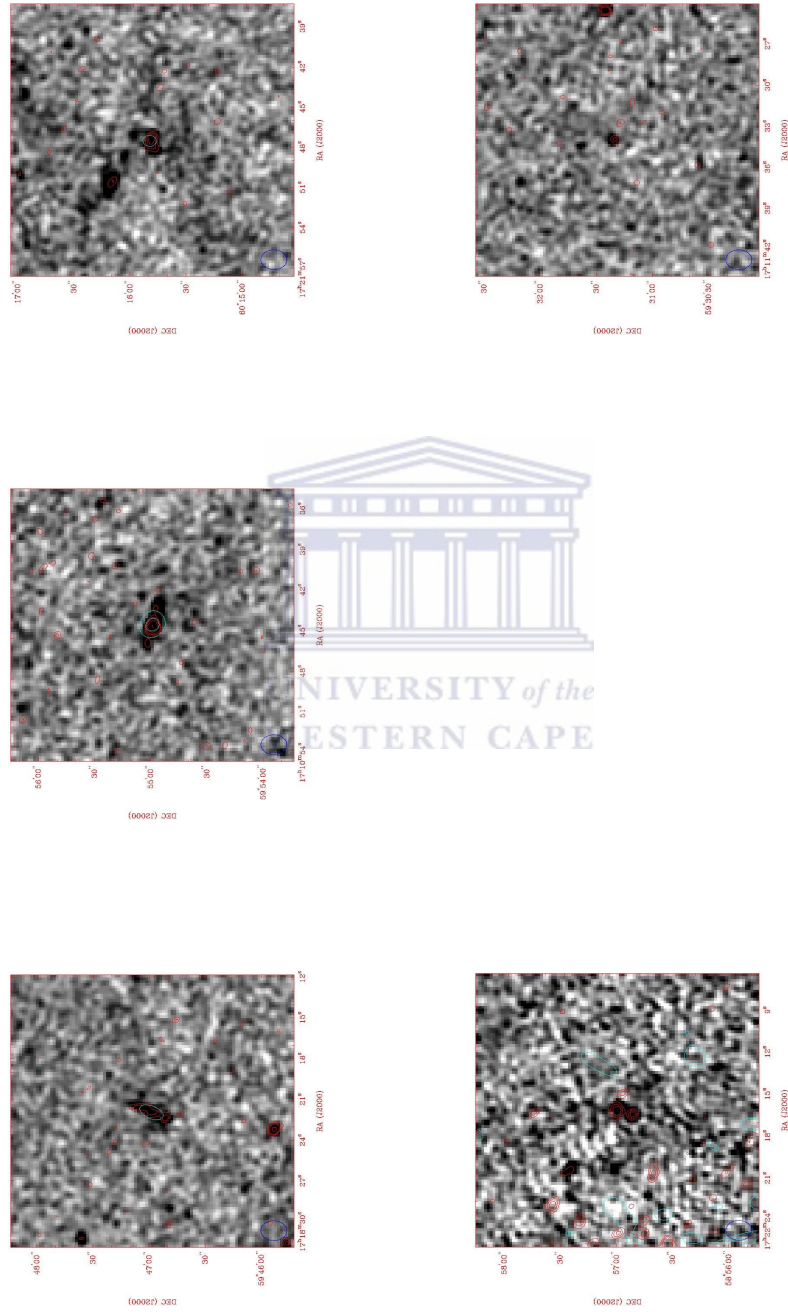
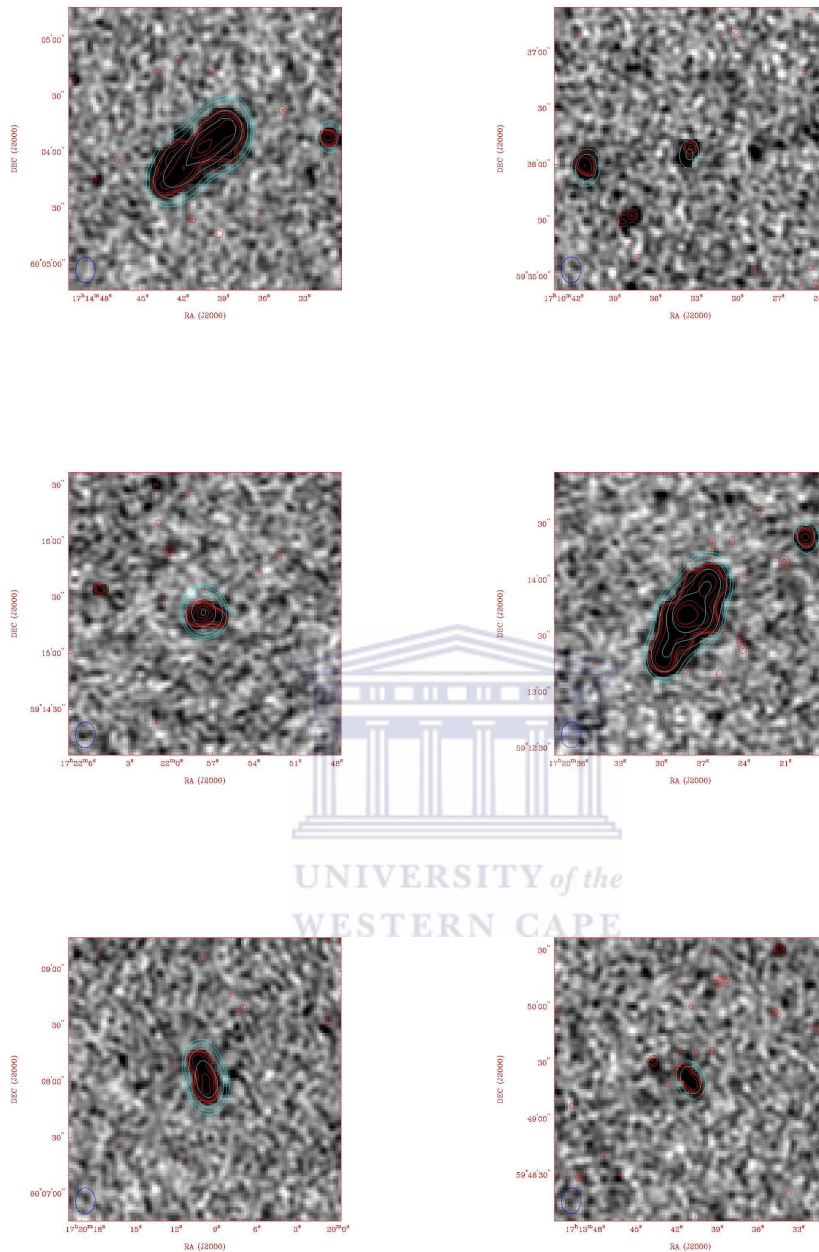


Figure 4.9: Continuation of Figure 4.7.



**Figure 4.10:** Radio images of sources having  $P_{1.4GHz} > 10^{24.5} W/Hz$ .

In order to enhance my morphological classification, I overlaid radio sources optically identified and deep NOAO optical images of the FLS field (Figure 4.11). It enabled me to check the position of the galaxy in the radio source. In Figure 4.11, the first row shows J172009.9+600802, J172027.9+591343 and J171440.2+600401. The last row shows J171409.4+590410 and J171821.9+594659. The grey scale is the opti-

cal image. The black contour is the VLA data and the outer level is  $80 \mu\text{Jy}$ .





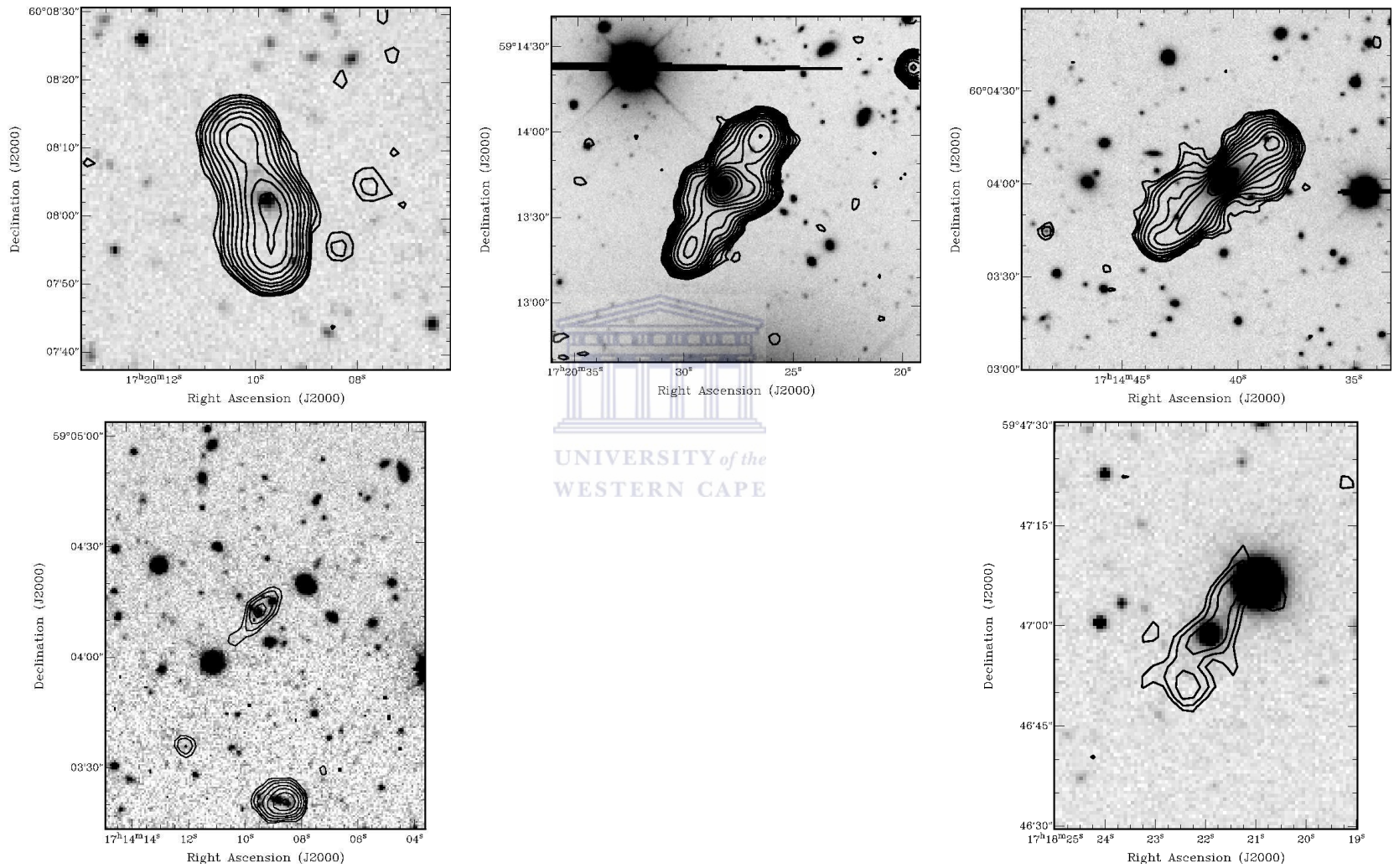


**Figure 4.11:** Overlay between radio sources optical identified and some deep NOAO optical image of the FLS field.

We note that two sources (J171440.2+600401 and J172157.7+591522 in Table 4.7) with FRI morphology appear to have the power of FRII galaxies, providing evidence that there is scatter in the correlation between power and morphology. Further optical data in the FLS field will allow a more complete sample for further investigation of this.





---

## Conclusions and recommendations

---

I have presented the results of an analysis of a sample of 107 multi-component radio sources from the FLS region obtained by cross-correlating the VLA and GMRT catalogues.

Visual inspection of the sample enabled me to make a preliminary classification of the sources in Fanaroff and Riley Class I/II, Peculiar, Compact, Extended, etc., according to their morphology.

In my analysis of spectral indices, I found that the majority of multi-component sources are steep-spectrum sources, Nevertheless the spread in the spectral distribution is wide, with a significant number of ultra, flat or inverted sources in agreement with Prandoni et al. (2009). This indicates the presence of an heterogeneous population, consisting of a mixture of flat/steep-spectrum AGNs and steep star-forming galaxies (Prandoni et al., 2009). The wide range of spectral indices could also indicate a wider range of accretion mechanisms in the sub-mJy sample. On the other hand, the ultra-steep spectrum sources ( $\alpha < -1.3$ ) present in the sample, if real, could potentially be associated with very high redshift galaxies (Prandoni et al., 2006).

Cross-correlating my sample of 107 multi-component radio sources with the Marleau et al. (2007) and Papovich et al. (2006) catalogues I obtained 23 optically identified sources with redshifts spanning the range  $0 < z < 1.8$  and peaking at  $z \sim 0.2$ . All identified objects are spectroscopically classified as galaxies. Some of them are classified as star-forming or star-burst galaxies, perhaps indicating that AGN and star-formation activity are ongoing in the same galaxy.

According to their radio power ( $P$ ), 6 of the identified objects are in the range of FR II sources ( $P_{1.4GHz} > 10^{24.5}W/Hz$ ) while 17 are in the range of FR I sources ( $P_{1.4GHz} < 10^{24.5}W/Hz$ ).

Combining radio images of all identified sources ordered by radio power, I found that most of sources having  $P_{1.4GHz} < 10^{24.5}W/Hz$  are compact and few are extended and peculiar, while all sources in the range of  $P_{1.4GHz} > 10^{24.5}W/Hz$  are extended.

The overlay between radio sources optically identified and deep NOAO optical image of the FLS field, gave me the position of the galaxy in the radio source. It enabled me to enhance the morphological classification of all sources optically identified. I found evidence for radio galaxies with FR II powers having FRI morphology.

Further optical follow-up is recommended to allow a more complete census of the sub-mJy population and more information on AGN feedback from such sources.



- Afonso, J., Mobasher, B., Koekemoer, A., Norris, R. P., and Cram, L. (2006). Optical and x-ray identification of faint radio sources in the goods cdf-s advanced camera for surveys field. *The Astronomical Journal*, 131:1216–1230.
- Alan, P. M., Svetlana, G. J., and et al. Francesca, D. D. (2008). The inner jet of an active galactic nucleus as revealed by a radio-to-gamma-ray outburst. *Nature*, 452:966–969.
- Arnold, T. J. and Martini, P. (2009). Active galactic nuclei in groups and clusters of galaxies: Detection and host morphology. *The Astrophysical Journal*, 707:1691–1706.
- Astron, N. I. R. A. (2009). Astron, netherlands institute for radio astronomy. <http://www.astron.nl/radio-observatory/astronomers/wsrt-astronomers>, accessed 2009 october 10.
- Baade, W. and Minkowski, R. (1954). Identification of the radio sources in cassiopeia, cygnus a, and puppis a. *Astrophysical Journal*, 119:206–214.
- Boucheffry, K. E. and Cress, C. M. (2006). Identifications of first radio sources in the noao deep-wide field survey. *Astronomische Nachrichten*, 999:789–797.
- Brookes, M. H., Best, P. N., Peacock, J. A., Röttgering, H. J. A., and Dunlop, J. S. (2008). A combined eis-nvss survey of radio sources (censors) - iii. spectroscopic observations. *Monthly Notices of the Royal Astronomical Society*, 385:1297–1326.
- Buttiglione, S., Capetti, A., Celotti, A., Axon, D. J., Chiaberge, M., Macchetto, D., and Sparks, W. B. (2009). An optical spectroscopic survey of the 3cr sample of radio galaxies with  $z < 0.3$ . ii. spectroscopic classes and accretion modes in radio-loud agn. *Astronomy & Astrophysics manuscript no. 13290*.

- Condon, J. J., Cotton, W. D., Yin, Q. F., Shupe, D. L., Storrie-Lombardi, L. J., Helou, G., Soifer, B. T., and Werner, M. W. (2003). The sirtf first-look survey. i. vla image and source catalog. *The Astronomical Journal*, 125:2411–2426.
- Dictionary, A. (2009). "spectral index." dictionary of astronomy. <http://www.encyclopedia.com>, accessed 2009 october 5.
- Edward, L. W. (2006). A cosmology calculator for the world wide web. *Astrophysical Journal (Draft)*.
- Fadda, D., Jannuzi, B. T., Ford, A., and Storrie-Lombardi, L. J. (2004). The spitzer space telescope first-look survey: Kpno mosaic-1 r-band images and source catalogs. *The Astronomical Journal*, 128:1–15.
- Fadda, D., Marleau, F. R., and and, L. J. e. (2006). The spitzer space telescope extragalactic first look survey: 24 microm data reduction, catalog and source identificatio. *The Astronomical Journal*, 131:2859–2876.
- Fanaroff, B. L. and Riley, J. M. (1974). The morphology of extragalactic radio sources of high and low luminosity. *Monthly Notices of the Royal Astronomical Society*, 167:31–36.
- Fang, F., Shupe, D. L., and et al. Wilson, G. (2004). The first measurements of galaxy clustering from infrared array camera (irac) data of the spitzer first look survey. *The Astrophysical Journal*, 154:35–38.
- Frayer, D. T., Fadda, D., and et al. Yan, L. (2006). Spitzer 70 and 160 m observations of the extragalactic first look survey. *The Astronomical Journal*, 131:250–260.
- Garn, T. and Alexander, P. (2008). Deep 610-mhz giant metrewave radio telescope observations of the spitzer extragalactic first look survey field - iii. the radio properties of infrared-faint radio sources. *Mon. Not. R. Astron. Soc.*, pages 1–9.
- Garn, T., Green, D. A., Hales, S. E. G., Riley, J. M., and Alexander, P. (2007). Deep 610-mhz gmrt observations of the spitzer extragalactic first look survey field - i. observations, data analysis and source catalogue. *Mon. Not. Roy. Astron. Soc.*, 376:1251–1260.

- Gonzalez-Solares, E. A., Perez-Fournon, I., and et al. Rowan-Robinson, M. (2005). The european large area iso survey: optical identifications of 15-*m* and 1.4-ghz sources in n1 and n2. *Mon. Not. R. Astron. Soc.*, 358:333–358.
- Haardt, F. and Maraschi, L. (1991). A two-phase model for the x-ray emission from seyfert galaxies. *Astrophysical Journal*, 380:51–54.
- Ivezic, Z., Menou, K., and et al. Strauss, M. (2002). Optical and radio properties of extragalactic sources observed by the first and sdss surveys. *Astronomical Journal*, 124:2364.
- Kantharia, N. G., Das, M., and Gopal-Krishna (2009). Gmrt detection of a new wide-angle tail (wat) radio source associated with the galaxy pgc 1519010. *Journal of Astrophysics and Astronomy*, 30:37–51.
- Kellermann, K. I. and Owen, F. N. (1988). *RADIO GALAXIES AND QUASARS*. 2nd edition.
- Klamer, I., Ekers, R., Bryant, J., Hunstead, R., Sadler, E., and De Breuck, C. (2006). Radio spectral energy distributions and the z-a correlation”. *MNRAS*, 371:852.
- Koulouridis, E., Plionis, M., V.Chavushyan, Dultzin, D., Krongold, Y., Georgantopoulos, I., and Goudis, C. (2009). The activity of the neighbours of agn and starburst galaxies: Towards an evolutionary sequence of agn activity, arxiv:0910.1355v1.
- Kraus, J. D. (1988). Grote reber - founder of radio astronomy. *R.A.S. Canada*, 82(3):107.
- Lacy, M., Wilson, G., Masci, F., Storrie-Lombardi, L. J., Appleton, P. N., Armus, L., Chapman, S. C., Choi, P. I., Fadda, D., Fang, F., Frayer, D. T., Heinrichsen, I., Helou, G., Im, M., Laine, S., Marleau, F. R., Shupe, D. L., Soifer, B. T., Squires, G. K., Surace, J., Teplitz, H. I., and Yan, L. (2005). The infrared array camera component of the spitzer space telescope extragalactic first look survey. *The Astrophysical Journal*, 161:41–52.
- Lilly, S. J. and Longair, M. S. (1984). Stellar populations in distant radio galaxies. *Royal Astronomical Society, Monthly Notices*, 221:833.

- Lyne, A. G., Graham-Smith, F., et al. (1998). *Pulsar Astronomy*. Cambridge Univ Pr, 2 edition.
- Magliocchetti, M., Andreani, P., and Zwaan, M. A. (2007). The radio properties of optically obscured spitzer sources. *Mon. Not. R. Astron. Soc.*, 383:479–496.
- Magliocchetti, M., Maddox, S. J., Wall, J. V., Benn, C. R., and Cotter, G. (2002). The redshift distribution of first radio sources at 1 mJy. *Monthly Notices of the Royal Astronomical Society*, 318:1047–1067.
- Manisha, J. (2009). Introducing gmrt: An illuminated gmrt antenna at twilight. [http://www.gmrt.ncra.tifr.res.in/gmrt\\_hpage/gmrt/intro\\_gmrt.html](http://www.gmrt.ncra.tifr.res.in/gmrt_hpage/gmrt/intro_gmrt.html), accessed 2009 october 10.
- Marleau, F. R., Fadda, D., Appleton, P. N., Noriega-Crespo, A., and Clancy, D. (2007). Spectroscopic survey of 1.4 ghz and 24 m sources in the spitzer first look survey with wiyh hydra. *The Astrophysical Journal*, 663:218–233.
- Maryam, H. (2009). An introduction to pulsars. <http://outreach.atnf.csiro.au/education/everyone/pulsars/>, accessed 2009 october 21.
- McCray, R. and Wang, Z. (1996). *Supernovae and supernova remnants: International Astronomical Union. Colloquium (145 : 1993 : Xian, China)*. Cambridge University Press.
- Mignano, A., Prandoni, I., Gregorini, L., Parma, P., de Ruiter, H. R., Wieringa, M. H., Vettolani, G., and Ekers, R. D. (2008). The atesp 5 ghz radio survey. ii. physical properties of the faint radio population. *Astronomy & Astrophysics manuscript*, (8545).
- Miley, G. and De Breuck, C. (2008). Distant radio galaxies and their environments. *A&ARv*, 15:67.
- Morganti, R., Garrett, M. A., Chapman, S., Baan, W., Helou, G., and Soifer, T. (2004). A deep wsrt 1.4 ghz radio survey of the spitzer space telescope flsv region. *Astronomy & Astrophysics*, 424:371–378.

- NASA, H. (2009). Introduction to supernova remnants. <http://heasarc.gsfc.nasa.gov/docs/objects/snrs/snrstext.html>, accessed 2009 october 20.
- Owen, F. N., Keel, W. C., Ledlow, M. J., Morrison, G. E., and Windhorst, R. A. (2005). A deep radio survey of abell 2125. i. radio, optical, and near-infrared observations. *A The Astronomical Journal*, 129:26–30.
- Owen, F. N. and Rudnick, L. (1976). Compact radio sources in the directions of rich clusters of galaxies. *Astrophysical Journal*, 203:307–312.
- Papovich, C., Cool, R., Eisenstein, D., Floc’H, E. L., Fan, X., Jr., R. C. K., Smith, J. D. T., Rieke, G. H., and Ard, M. V. (2006). A mmt/hectospec redshift survey of 24 micron sources in the spitzer first look survey. *Astronomical Journal*, 132:231–241.
- Pickering, T. E. (2009). The mmt observatory. <http://www.mmt.org/>, accessed 2009 october 20.
- Prandoni, I., Gregorini, L., Parma, P., de Ruiter, H. R., Vettolani, G., Wieringa, M. H., and Ekers, R. D. (2001). The atesp radio survey. iii. source counts. *Astronomy and Astrophysics*, 365:392–399.
- Prandoni, I., Morganti, R., and Mignano, A. (2009). The agn component in deep radio fields: Results from the first look survey. *Proceeding of Science*, *arXiv:0909.3761*.
- Prandoni, I., Parma, P., Gregorini, L., Mignano, A., Vettolani, G., and Ekers, R. D. (2006). The atesp 5 ghz radio survey i. source counts and spectral index properties of the faint radio population. *Astronomy & Astrophysics*, 457:517.
- Robyn, H. (2009). An overview of the very large array. <http://www.vla.nrao.edu/genpub/overview/>, accessed 2009 october 10.
- Rohlfs, K. and Wilson, T. (2003). *Tools of Radio Astronomy*. 4th revised and enlarged edition.
- Ryle, M. and Sandage, A. (1964). The optical identification of three new radio objects of the 3c 48 class. *Astrophysical Journal*, 139:419.

- Sadler, E., Jackson, C., and et al. Cannon, R. (2002). Radio sources in the 2df galaxy redshift survey - ii. local radio luminosity functions for agn and star-forming galaxies at 1.4ghz. *Mon. Not. R. Astron. Soc.*, 329:227.
- Seyfert, C. K. (2007). Nuclear emission in spiral nebulae. *Astrophysical Journal*, 97:28.
- Smith, F. G. (1951). *Nature*, 168:555.
- Smith, F. G. (1952). *Mon. Not. Roy. Astron. Soc.*, 112:497.
- Smits, R., Kramer, M., Stappers, B., Lorimer, D., Cordes, J., and Faulkner, A. (2008). Pulsar searches and timing with the ska, arxiv:0811.0211v1. *Astronomy & Astrophysics*.
- Snellen, I. A. G. and Best, P. N. (2001). Distant *fri* radio galaxies in the hubble deep field: implications for the cosmological evolution of radio-loud agn. *Mon. Not. R. Astron. Soc.*, 328:897–902.
- Sparke, L. S. and Gallagher, J. S. (2007). *Galaxies in the Universe: An Introduction*. Cambridge: Cambridge University Press.
- Stoughton, C., Lupton, R. H., and et al. Bernardi, M. (2002). Sloan digital sky survey: Early data release. *The Astronomical Journal*, 123:485–548.
- Sullivan, M., Hopkins, A. M., Afonso, J., Georgakakis, A., Chan, B., Cram, L. E., Mobasher, B., and Almeida, C. (2004). The phoenix deep survey: Optical and near-infrared imaging catalogs. *The Astrophysical Journal*, 155:1–13.
- Sutherland, W. and Sanders, W. (1992). Lrt for source identification. *Monthly Notices of the Royal Astronomical Society*, 259:413.
- Tony, G. and Martin, P. (2009). About spitzer. <http://www.spitzer.caltech.edu/about/index.shtml>, accessed 2009 october 10.
- Whiting, M. T. (2005). On the nature of bl lac objects. *Mom. S. A. It.*, 76:61.
- Willott, C. J., Delorme, P., and et al. Omont, A. (2007). Four quasars above redshift 6 discovered by the canada-france high-z quasar survey. *The Astronomical Journal*, 134:2435–2450.



- Wiyun, O. (2009). Wiyun observatory. <http://www.noao.edu/wiyun/>, accessed 2009 october 10.
- Young, D. S. D. (2002). *The Physics of Extragalactic Radio Sources*. The University of Chicago Press.
- Young, M., Manchester, R., and Johnston, S. (1999). A radio pulsar with an 8.5-second period that challenges emission models. *Nature*, 400:848–849.

